Cellular/Molecular

Synapse-Enriched m^{6}A-Modified Malat1 Interacts with the Novel m^{6}A Reader, DPYSL2, and Is Required for Fear-Extinction Memory

Sachithrani U. Madugalle,[1*] Wei-Siang Liau,[1*] Qiongyi Zhao,[1*] Xiang Li,[2,3] Hao Gong,[1] Paul R. Marshall,[1] Ambika Periyakaruppiah,[1] Esmi L. Zajaczkowski,[1] Laura J. Leighton,[1] Haobin Ren,[1] Mason R. B. Musgrove,[1] Joshua W. A. Davies,[1] Gwangmin Kim,[1] Simone Rauch,[4] Chuan He,[4] Bryan C. Dickinson,[4] Barbora Fulopova,[1] Lee N. Fletcher,[1] Stephen R. Williams,[1] Robert C. Spitale,[5] and Timothy W. Bredy[1]

[1]Queensland Brain Institute, University of Queensland, Brisbane, Queensland, Australia 4072, [2]Department of Neurosurgery, Zhongnan Hospital of Wuhan University, Wuhan, China 430071, [3]Medical Research Institute, Wuhan University, Wuhan, China 430014, [4]Department of Chemistry, University of Chicago, Chicago, Illinois 60607, and [5]Department of Pharmaceutical Sciences, University of California–Irvine, Irvine, California 92697

The RNA modification N^6-methyladenosine (m^{6}A) regulates the interaction between RNA and various RNA binding proteins within the nucleus and other subcellular compartments and has recently been shown to be involved in experience-dependent plasticity, learning, and memory. Using m^{6}A RNA-sequencing, we have discovered a distinct population of learning-related m^{6}A- modified RNAs at the synapse, which includes the long noncoding RNA metastasis-associated lung adenocarcinoma transcript 1 (*Malat1*). RNA immunoprecipitation and mass spectrometry revealed 12 new synapse-specific learning-induced m^{6}A readers in the mPFC of male C57/BL6 mice, with m^{6}A-modified *Malat1* binding to a subset of these, including CYFIP2 and DPYSL2. In addition, a cell type- and synapse-specific, and state-dependent, reduction of m^{6}A on *Malat1* impairs fear-extinction memory; an effect that likely occurs through a disruption in the interaction between *Malat1* and DPYSL2 and an associated decrease in dendritic spine formation. These findings highlight the critical role of m^{6}A in regulating the functional state of RNA during the consolidation of fear-extinction memory, and expand the repertoire of experience-dependent m^{6}A readers in the synaptic compartment.

Key words: epitranscriptomic; long noncoding RNA; m6A reader; memory; RNA m6A; synapse

Significance Statement

We have discovered that learning-induced m^{6}A-modified RNA (including the long noncoding RNA, *Malat1*) accumulates in the synaptic compartment. We have identified several new m^{6}A readers that are associated with fear extinction learning and demonstrate a causal relationship between m^{6}A-modified *Malat1* and the formation of fear-extinction memory. These findings highlight the role of m^{6}A in regulating the functional state of an RNA during memory formation and expand the repertoire of experience-dependent m^{6}A readers in the synaptic compartment.

Received May 22, 2023; revised Aug. 29, 2023; accepted Aug. 29, 2023.

Author contributions: S.U.M., S.R.W., R.C.S., and T.W.B. designed research; S.U.M., W.-S.L., X.L., H.G., P.R.M., A.P., E.L.Z., L.J.L., H.R., M.R.B.M., J.W.A.D., G.K., B.F., and L.N.F. performed research; S.U.M., Q.Z., P.R.M., B.F., and L.N.F. analyzed data; S.U.M. wrote the first draft of the paper; S.U.M., R.C.S., and T.W.B. edited the paper; W.-S.L., X.L., S.R., C.H., B.C.D., and S.R.W. contributed unpublished reagents/analytic tools; T.W.B. wrote the paper.

This work was supported by National Institutes of Health R01MH109588 to T.W.B. and R.C.S.; National Health and Medical Research Council Ideas Grant GNT2003414 to T.W.B.; National Natural Science Foundation of China 82001421; National Institutes of Health, National Institute of General Medical Sciences R35 GM119840 to B.C.D.; and ARC LIEF Grant LE100100074. E.L.Z, L.J.L., and S.U.M. were supported by Westpac Future Leaders Scholarships and the University of Queensland. We thank Dr. Alun Jones (Mass Spectrometry Facility in the Institute for Molecular Bioscience, University of Queensland) for help with the proteomics experiments; and Rowan Tweedale (Queensland Brain Institute) for help in manuscript editing.

*S.U.M., W.-S.L., and Q.Z. contributed equally to this work.

C.H. is a scientific founder and a member of the scientific advisory board of Accent Therapeutics Inc. and Inferna Green Inc. B.C.D. is a founder and holds equity in Tornado Bio, Inc. The remaining authors declare no competing financial interests.

Correspondence should be addressed to Timothy W. Bredy at t.bredy@uq.edu.au.

https://doi.org/10.1523/JNEUROSCI.0943-23.2023

Introduction

The extinction of conditioned fear, the reduction in responding to a feared cue, which occurs when the cue is repeatedly presented without any adverse consequence, is an evolutionarily conserved behavioral adaptation that is critical for survival. Like other forms of learning, long-lasting memory for fear extinction depends on coordinated changes in gene expression, particularly in the infralimbic PFC (ILPFC) (Martin et al., 2000; Bruel-Jungerman et al., 2007; Alberini, 2009). We and others have shown that this process involves a variety of RNA-based mechanisms, including the activity of microRNAs (Lin et al., 2011) and the localized regulation of transcription by long noncoding RNAs (lncRNAs) (Barry, 2014; Spadaro et al., 2015; Wei et al., 2022). However, other mechanisms can also influence RNA metabolism and the capacity of neurons to adapt in response to learning. In particular, the RNA

modification N6-methyladenosione (m^{6}A) is dynamic and reversible (Jia et al., 2011) and regulates many aspects of state-dependent RNA metabolism in the CNS, including RNA stability, localization, and translation (Shi et al., 2018; J. Zhou et al., 2018; Madugalle et al., 2020). This epitranscriptomic mark is enriched in the adult rodent brain (Meyer et al., 2012), and is directly involved in dopaminergic signaling (Hess et al., 2013; Bai et al., 2018; X. Chen et al., 2019), spatial memory consolidation (Walters et al., 2017; Z. Zhang et al., 2018), and the acquisition of fear-related learning and memory (Widagdo et al., 2016). In addition, synapse-enriched m^{6}A-modified RNA has recently been discovered in the adult brain (Merkurjev et al., 2018); however, the functional relevance of synaptically localized m^{6}A-modified RNAs and their interacting partners in the context of fear extinction has not been elucidated.

Many RNA binding proteins (RBPs) recognize and interact with m^{6}A-modified RNA; and several, including the YTHDF family of proteins, have been shown to be m^{6}A readers (Alarcón et al., 2015; Wang et al., 2015; Xiao et al., 2016; Roundtree et al., 2017; Edens et al., 2019; Fu and Zhuang, 2020). However, whether there are m^{6}A readers in the synaptic compartment that support specific forms of learning and memory, including fear-extinction, is unknown. Given the increasing recognition that m^{6}A-modiifed RNAs play important roles in brain function (Madugalle et al., 2020), we investigated their impact on this important learning process. Using RNA immunoprecipitation followed by mass spectrometry, we discovered 12 novel extinction learning-induced m^{6}A readers that are primarily associated with synaptic remodeling and synaptic vesicle endocytosis. This was accompanied by the detection of a unique population of learning-related m^{6}A-modified RNAs at the synapse, including the lncRNA metastasis-associated lung adenocarcinoma transcript 1 (*Malat1*). Our results revealed that m^{6}A-modified *Malat1* interacts with a subset of novel m^{6}A readers, including cytoplasmic FMR1 interacting protein 2 (CYFIP2) and dihydropyrimidase-related protein 2 (DPYSL2, otherwise known as CRMP2), and demonstrates that both targeted degradation and demethylation of m^{6}A-modified *Malat1* at the synapse impair fear-extinction memory. The formation of fear-extinction memory therefore relies on a direct interaction between m^{6}A-modified *Malat1* and a select number of novel m^{6}A readers in the synaptic compartment.

Materials and Methods

Animals. Adult, male C57BL/6J mice (9-10 weeks old, 20-25 g) supplied from the Animal Resources Center were used for experiments. Mice were housed 4 animals per cage on a 12 h light:dark cycle (lights on 0700 h) in a humidity- and temperature-controlled vivarium, with rodent chow and water provided *ad libitum*. All procedures were conducted according to protocols and guidelines approved by the University of Queensland Animal Ethics Committee.

Lentiviral surgery. Double cannulae (PlasticsOne) were implanted in the anterior posterior plane, along the midline into the ILPFC. The injection coordinates were centered at 1.85 mm in the AP plane and −2.8 mm in the DV plane. Following surgery, animals were given at least 1 week to recover before lentivirus infusions. A total of 2 µl of lentivirus (with a titer from 1×10^7 to 1×10^8 IU/ml) was introduced via two injections, delivered at a rate of 0.1 µl/min, 48 h apart. Animals were fear conditioned 24 h before lentiviral infusions and 1 week after lentiviral infusions mice were extinction trained.

Behavioral tests. All behavioral testing was conducted during the light phase in red-light-illuminated testing rooms. Two contexts (A and B) were used for all behavioral fear testing. Both conditioning chambers (Coulbourn Instruments) had two transparent walls and two stainless-steel walls with a steel grid floor (3.2 mm in diameter, 8 mm centres); however, the grid floors in Context B were covered by a flat white plastic transparent surface. This surface was used to minimize context generalization. Digital cameras were mounted in the ceiling of each chamber and connected via a quad processor for automated scoring in a freezing measurement program (FreezeFrame). Fear conditioning (Context A) was performed with a spray of lemon-alcohol (5% lemon and 10% alcohol). The fear-conditioning protocol started with a 120 s pre-fear-conditioning habituation period, which was followed by three pairings of a 120 s, 80 dB white noise conditioned stimulus (CS) with a 1 s, 0.7 mA foot shock unconditioned stimulus (US). Based on freezing percentages, mice were matched into equivalent treatment groups (*Malat1* virus or control virus). For extinction (EXT, Context B), which was performed with a spray of vinegar, mice were again allowed to acclimate for 2 min, after which they were extinction trained using 60 nonreinforced 120 s CS presentations (a 60CS training protocol). For the control experiments, animals did not receive the CS (this group is known as the retention control [RC]). Memory was tested by returning animals to Context B (24 h apart) with a 3CS-only presentation. In these tests, the CS was presented, but no foot shock (US) was delivered. Memory was calculated as the percentage of time spent freezing during the tests.

Synaptosome isolation. Synaptosomes were isolated from the mPFCs of behaviorally trained adult mice using a discontinuous Percoll-sucrose density gradient with modifications. For tissue collection for synaptosome isolations, 24 mice were fear-conditioned, after which 12 were taken as RC and 12 were 60 CS extinction trained, 24 h later. Immediately after extinction training, the animals were cervically dislocated; and mPFC was dissected from the whole brain, snap frozen on liquid nitrogen, and transferred to −80°C storage. For one synaptosome isolation, four PFCs were homogenized in ice-cold GM buffer (2.5 M sucrose, 1 M Tris-HCl), leaving 3 RC and 3 EXT samples. The homogenate was centrifuged at $1000 \times g$ for 10 min at 4°C, to pellet the nuclei, and the supernatant was applied to a discontinuous Percoll gradient, comprising 3%, 10%, 15%, and 23% Percoll layers (GE Healthcare) in GM buffer and RNaseOUT (1:1000, Fisher Scientific). Therefore, each replicate had nonsynaptic and synaptic fractions for subsequent experiments. The gradient was centrifuged at 18,400 rpm for 5 min at 4°C in a fixed-angle rotor. Four major fractions were separated from the Percoll gradient, with synaptosomes being collected from layers 3 and 4. These layers were pooled for each sample, diluted fourfold with cold GM buffer, and pelleted by centrifuging at 14,800 rpm for 30 min at 4°C. The pellet was transferred to a new tube and stored at −80°C until ready for use.

RNA extraction. For all samples (from neuronal cultures and PFC nonsynaptic and synaptic fractions), RNA was extracted using NucleoZOL reagent (Scientifix), as per the manufacturer's protocol. At the phase separation step, where the nuclei and protein were pelleted, the supernatant was combined with an equal volume of 95%-100% ethanol and transferred to a RCC5 column (part of the RNA Clean and Concentrator kit from Zymo Research), and the manufacturer's instructions were followed. RNA was eluted in 20 µl of water and used for qRT- PCR or low-input sequencing (described below).

qRT-PCR. Up to 1 µg RNA was used for cDNA synthesis using the Quantitect Reverse Transcription Kit (QIAGEN). qPCR was performed on a RotorGeneQ (QIAGEN) using SYBR-Green Master Mix (QIAGEN), with primers for target genes (*Malat1* Peak 1 forward: 5′-CTTCCTAC TACCTGTGCCTTTAAG-3′, *Malat1* Peak 1 reverse: 5′-AAGTGTTAG GCTAGCCGGGC-3′, *Malat1* Peak 2 forward: 5′-CGCAGTTGACA AGCCAAGC-3′, *Malat1* Peak 2 reverse: 5′-GCATTGGACTTGAGCTG AGG-3′, *Malat1* Peak 3 forward: 5′-CTTCCTACATTCCCACCCAG CAC-3′, *Malat1* Peak 3 reverse: 5′-GAGGTCACGTTGCATATCGG-3′, *Homer1* forward: 5′-CTGACCAGTACCCCTTCACAG-3′, *Homer1* Reverse: 5′-CCAAGTTTCACTCTGGCACAAA-3′, *Hsp90ab1* forward: 5′-AGTACTTGGAGGAGAGGAGGG-3′, *Hsp90ab1* reverse: 5′-GGTGATGGGATAGCCTATGAACTG-3′) on a RotorGeneQ real-time PCR cycler. All transcript levels were normalized to input RNA using the % input method, and each PCR was run in triplicate for each sample.

Low-input m^{6}A sequencing. RNA extracted from nonsynaptic and synaptic mPFC fractions was used for m^{6}A RNA immunoprecipitation

(RIP) as previously described (Dominissini et al., 2012) with slight modifications. Up to 100 ng of nonsynaptic and synaptic RNA was used. The RNA was chemically fragmented into ~100 nucleotide fragments by 5 min incubation at 94°C in fragmentation buffer (10 mM $ZnCl_2$, 10 mM Tris-HCl, pH 7), after which the fragmentation was stopped with 0.05 M EDTA. Input samples were stored at −80°C. m^{6}A-enriched samples were incubated overnight at 4°C with 5 µg of affinity purified anti-m^{6}A polyclonal antibody (Abcam) in IPP buffer (150 mM NaCl, 0.1% NP-40, 10 mM Tris-HCl, pH 7.4). The mixture was then immunoprecipitated by incubation with Dynabeads Protein-G beads (Fisher Scientific) at 4°C for 2 h. After extensive washing, bound RNA was eluted from beads in 10 µl of water; 8 µl of RNA was used for library generation with the SMARTer Stranded Pico Input Mammalian Takara kit, according to the manufacturer's instructions. Each library was subjected to AMPure XP (Beckman Coulter) purification to remove primer-dimers and fragments >500 bp. The final libraries (size distribution from 200 to 500 bp, with the peak at ~400 bp) were run on a single-flow cell on HiSeq 4000 (Illumina) for paired-end sequencing.

For m^{6}A enrichment of RNA for qRT-PCR, there were four groups of RNA: input, m^{6}A enriched, unmodified RNA, or IgG control. RNA was not fragmented. An overnight incubation was also conducted with either the anti-m^{6}A antibody or mouse IgG control antibody (Santa Cruz Biotechnology). The supernatant or "unmodified" RNA fraction (i.e., the RNA that did not bind to the m^{6}A antibody conjugated beads) was also saved (for antibody details, see Table 1). All samples were washed and eluted in 12 µl of water and used for cDNA synthesis.

m^{6}A sequencing data analysis. Cutadapt (version 1.17) was used to trim off low-quality nucleotides (Phred quality <20) and adaptor sequences at the 3′ end. All reads were aligned against the ribosome RNA and PhiX reference sequences using bowtie2 (version 2.3.4.2). Reads that could be aligned to either the ribosome RNA or the PhiX reference were removed. HiSAT (version 2.1.0) was then used to align the filtered reads against the mouse genome reference (mm10). After the alignment, SAMtools (version 1.8) was used to remove the duplicate reads (with the option of "markup -r"), and subsequently extract the properly paired and high-quality aligned reads (with the option of "- f2-q 20") for downstream analyses. Significantly m^{6}A-modified transcripts in the RC versus EXT groups were determined using ExomePeak (version 2.16.0). In exomePeak's algorithm, the *p* value was calculated based on Przyborowski and Wilenski's method for comparing the means of two Poisson distributions (C test) (Przyborowski and Wilenski, 1940; Krishnamoorthy and Thomson, 2004), and the false discovery rate was calculated by switching the case and control samples (Meng et al., 2013). These transcripts were used in Gene Ontology (GO) functional analysis using the DAVID Bioinformatic Resources. The Integrative Genomics Viewer software (version 2.7.2) was used to view m^{6}A peaks in each sample.

Neuronal cell culture. Cortical neurons from embryonic day 16 (E16) mice were prepared and maintained in neurobasal medium containing 2% B28, 2 mM Glutamax, 50 U/ml penicillin, and 50 µg/ml streptomycin. Neurons were transduced with lentivirus at 3 DIV and harvested for experiments at 10 DIV, after a 4 h, 20 mM KCI stimulation. For the RNA BaseScope, cortical neurons were plated in Nunc Lab-Tek II 4-well chamber slides (Fisher Scientific) coated with poly-ornithine, harvested at 7 DIV, and labeled under baseline conditions (i.e., no KCI stimulation).

RNA BaseScope. On DIV 7, primary cortical neurons were washed with 1× PBS for 2 min, followed by a 30 min 10% formalin fixation. After fixation, slides were washed with 1× PBS and the chamber slide disassembled to remove the outer casting. Next, each well was barriered by drawing around the well with a hydrophobic barrier pen (ImmEdge), after which 50 µl of 1:15 protease III (diluted in PBS) from the BaseScope kit was applied to the slides, incubated for 8 min in a humidity tray at room temperature, and rinsed with 1× PBS. Slides were then incubated with either the negative or *Malat1* probe for 2 h at 40°C. The negative probe targeted the dihydrodipicolinate reductase (*DapB*) gene from *Bacillus subtilis* (a bacterial enzyme) (Grabinski et al., 2015). The *Malat1* probe was designed at chr19: 5797504-5797533. The probe signal was amplified by applying 50 µl of eight different "AMP" solutions to each well, one at a time in numerical order, with 40°C incubation for 15 (AMP 3, 6, 8) or 30 (AMP 1, 2, 4, 5, 7) min. Between each AMP solution, slides were rinsed with 1× PBS. After incubating in AMP8, 50 µl of BaseScope Fast Red solution (1:60 ratio of Solution B to Solution A) was applied, avoiding light exposure. Slides were then washed with 1× PBS with 0.3% Triton-X 100 (PBST) and blocked using blocking buffer (5% goat serum, 0.3% Triton X-100 in 1× PBS) for 1 h at room temperature. After blocking, neurons were incubated overnight (4°C on a shaker) in primary MAP2 antibody (Abcam) to label the morphology of neurons. After the overnight incubation, slices were washed 3 times PBST, for 5 min per wash. After the final wash, secondary GFP antibody (Fisher Scientific) diluted in blocking buffer was added to the cells, after which they were washed using 1× PBST, 3 times, at 5 min per wash and then stained with DAPI (1:2000 dilution in 1× PBST, 5 min). DAPI staining was followed by a 2 min 1× PBS wash. DAKO fluorescence mounting medium was added to cover the slide before coverslipping. The slides were imaged using an LSM510 confocal microscope and Zeiss ZEN Microscopy Software.

Table 1. Antibodies used for m^{6}A-RIP, IHC, and fRIP-qPCR[a]

Antibody	Type	Company	Dilution/ concentration
m^{6}A	Mouse monoclonal	Active motif	5 µg
IgG	Mouse polyclonal	Diagenode	5 µg
Anti-CYFIP2	Mouse monoclonal	Santa Cruz Biotechnology	5 µg
Anti-CRMP2	Mouse monoclonal	Santa Cruz Biotechnology	5 µg
Anti-GFP	Rabbit polyclonal	Abcam	1:2000
Anti-MAP2	Chicken polyclonal	Abcam	1:5000
Rabbit IgG	Rabbit polyclonal	CST	1:2000
Chicken IgG	Chicken polyclonal	Bio-Rad	1:5000
Goat anti-rabbit (488 nm)	Rabbit polyclonal	Invitrogen	1:1000
Goat antirchicken (647 nm)	Chicken polyclonal	Invitrogen	1:1000

[a]List of antibodies with manufacturer and concentration/dilution details used for all experiments.

RNA immunoprecipitation and mass spectrometry. Control (biotin-AUGGGCCGUUCAUCUGCUAAAAGGACUGCUU UUGGGGCUU GU) and m^{6}A (biotin-AUGGGCCGUUCAUCUGCUAAAAGG-m^{6}A-CUGCUUUUGGGGCUUGU) previously published biotin-labeled RNA oligonucleotides were used in this assay (Dominissini et al., 2012). Streptavidin-conjugated agarose beads (Fisher Scientific) were preblocked using 1% BSA for 30 min at 4°C, after which the BSA was discarded and the beads were resuspended in 1× RNA capture buffer (20 mM Tris, pH 7.5, 1 M NaCl, 1 mM EDTA, 1 µl RNaseOUT) and 2 µg of oligonucleotides was added per reaction. The beads and oligonucleotides were then incubated for 2 h at 4°C, after which the beads were washed 3 times with 20 mM Tris, pH 7.5, at 5-10 min per wash; 1× protein-RNA binding buffer (20 mM Tris, pH 7.5, 50 mM NaCl, 2 mM $MgCl_2$, 0.1% Tween-20, 100 U/ml RNAseOUT, 1 M DTT, 1× PIC) was then added to the beads and maintained at 4°C until lysates were prepared. Nonsynaptic and synaptic lysates from trained mouse PFC tissue were washed with 1× PBS (8000 rpm, 2 min, 4°C). Lysates were resuspended in RNA immunoprecipitation buffer (150 mM KCI, 25 mM Tris, pH 7.4, 5 mM EDTA, 0.5 mM DTT, 0.5% NP40, 100 U/ml RNAseOUT, 1 M DTT, 1× PIC) and incubated on ice for 30 min. Lysates were then centrifuged for 15 min at 10,000 × *g* (4°C), after which the supernatant was transferred to a new tube and protein-RNA binding buffer with 30 µl of 50% glycerol was added to each lysate. These lysates were then incubated with prebound beads and oligonucleotides 2 h at 4°C and then UV crosslinked for 2 min at 120,000 kJ. After crosslinking, beads were washed 2-3 times with wash buffer (20 mM Tris, pH 7.5, 10 mM NaCl, 0.1% Tween-20, RNAseOUT, 1 M DTT, 1× PIC) for 5 min per wash. After the last wash, the beads were sent for liquid chromatography-mass spectrometry. Three replicates were conducted for each group (RC-control, RC-m^{6}A, EXT-control, and EXT-m^{6}A). The same method was used for the *Malat1* protein-pull down assay, but this time using probes against *Malat1* (CTGAGTGTTGAGGAAAT GGCTCTCTGCAGC). For the *Malat1* RIP-MS, instead of a control oligonucleotide, a sample with all the synaptic proteins (i.e., "synaptic input")

Table 2. CIRTS PCR cloning primers[a]

Name	Primer sequence
AgeICirts6-9-11gRNA forward	ATACCGGTATGGGAATTATCAACACC
XbaINheICirts reverse	GCTCTAGACTGGGCTAGCTCCCCAGCATGCCTGC
NheICalm3 forward	CTAGCTAGCGAAGTCGGTCCGGATTCC
XbaICalm3 reverse	GCTCTAGAAACTCTAGGGGGTTCCGA
XbaIU6 forward	GCTCTAGAGAGGGCCTATTTCCCATG
XbaIBsmBIgRNA reverse	GCTCTAGACGTCTCAAAAAAGCGTCTCAATAAGGCCAGAGAGCTCC
NheIDF2 reverse	CTAGCTAGCCTACTTGTCATCGTCGTC
Peak 1 reverse	CAAAAAAAAAAACAAAAAGGTTAGGC
Peak 2 reverse	CAAAAACCAGTTTGGTGAAG
Peak 3 reverse	CAAAAACCCTTGCCTGTAATTTAAC

[a]Sequences of primers used for constructing CIRTS-YTHDF2 and CIRTS-FTO plasmids.

was used, where high confidence *Malat1* proteins which overlapped with high confidence synaptic proteins were determined to be the proteins which interacted with *Malat1* at the synapse in the RC and EXT groups. Each group was manually sorted for high confidence proteins which was a two-step sorting process. First, in each replicate, if two or more peptides were detected per protein, these proteins were used to compare between replicates. If proteins (with two or more peptides) were present in two or more replicates, these proteins were classified as high confidence proteins per group. All proteins were analyzed by STRING to determine functional protein association networks and clusters.

Cloning. The CRISPR-Cas-Inspired RNA Targeting System (CIRTS) was used to demethylate or degrade modified RNA because it is a single construct for which the protein component is much smaller than earlier iterations of CRISPR-Cas (Rauch et al., 2019). The pFsy(1.1)GW lentiviral expression vector (Addgene #27232), containing the synapsin 1 (Syn1) promoter, was used to make the Syn1-CIRTS-Calm3 construct. Upon synaptic activity, it has been demonstrated that STAUFEN binds to the 3′ untranslated region (3′UTR) of *Calm3* to mediate the localization of *Calm3* to dendrites (Sharangdhar et al., 2017). Therefore, after transcription of the CIRTS components and neuronal activation, the addition of *Calm3* allows the entire construct to be localized to the synapse. As the guide is expressed everywhere, the construct can then be used to degrade/demethylate m^{6}A-*Malat1* at the synapse.

The CIRTS PIN nuclease construct, containing a C-terminal Flag tag and nuclear export signal, was a kind gift from the group of Prof Bryan Dickinson. The CIRTS cassette was PCR amplified and cloned into the AgeI and XbaI sites. An NheI site was generated upstream of XbaI using PCR primer. The Calm3 dendritic localization sequence was PCR amplified from psiCheck2-Calm3 (a kind gift from Prof Michael Kiebler) and cloned into the NheI and XbaI sites. Finally, the U6-guide RNA (gRNA) scaffold was PCR amplified from the CIRTS PIN nuclease construct and inserted in the XbaI site to make the final construct (for PCR cloning primer sequences, see Table 2). For the CIRTS YTHDF2 Calm3 plasmid, the above Syn1-CIRTS-Calm3 construct was digested using AgeI and NheI. The original CIRTS-6, B- defensin 3-TBP6.7-YTHDF2 plasmid (#132544), was purchased from Addgene and the YTHDF2 domain was PCR amplified and cloned into the AgeI and NheI sites. The CIRTS-FTO plasmid was constructed similarly, using the full-length FTO sequence synthesized by IDT. GFP was PCR amplified and cloned into the AgeI site together with a 2A peptide signal.

Finally, to clone the gRNAs into the plasmids, DNA fragments were synthesized by IDT. Three gRNAs against *Malat1* (corresponding to m^{6}A peaks identified in Fig. 1) or a control guide were cloned into the constructs to generate three individual *Malat1* targeting constructs and one control construct. Each guide had the U6 promoter (with the XbaI site), followed by TBP fold (RNA hairpin binding domain), guide sequence, and overhang with an EcoRI site. Guides were PCR amplified and cloned into the plasmid using XbaI and EcoRI sites (Table 3).

Immunohistochemistry. At the end of testing, animals in the RC groups were killed and 1× PBS was pumped through the circulatory system, followed by 4% PFA to fix the tissue. The brains were sectioned at 50 µm using a vibratome. Slices were collected into PBS, then blocked using blocking buffer (5% goat serum, 0.3% Triton X-100 in 1× PBS) for 1 h at room temperature. After blocking, primary antibody was diluted in blocking buffer and incubated with the slices overnight at 4°C on a shaker. The slices were then washed 3 times with 1× PBST for 5 min per wash. After the final wash, secondary antibody diluted in blocking buffer was added and incubated at room temperature for 1.5 h. The slices were subsequently washed using 1× PBST, 3 times, at 5 min per wash and then stained with DAPI (1:2000 dilution in 1× PBST, 5 min). DAPI staining was followed by a 2 min 1× PBS wash. Slices were transferred onto a glass slide, and DAKO fluorescence mounting medium was added to cover the slide before coverslipping. Slides were dried completely overnight before imaging using confocal microscopy and image analysis using ZEN2012.

Similarly, to visualize the CIRTS construct in primary cortical neurons, lentivirus was transduced 2 d post-plating on glass poly-D-lysine-coated coverslips. Seven days later, cells were fixed with 4% PFA for 10 min at room temperature, washed for 5 min with 100 mM glycine in PBS to quench the reaction, then washed 3 times with 1× PBS, at 5 min per wash. Fixed cells were permeabilized by incubating in 0.4% Triton X-100 in 1× PBS for 15 min at room temperature and immunohistochemistry was continued as above.

SELECT assay. The single-base elongation and ligation-based PCR amplification method to detect m^{6}A along *Malat1* was conducted as previously described (Xiao et al., 2018). DNA oligonucleotides were designed either side of the three m^{6}A sites along *Malat1* that were targeted by the CIRTS construct (for sequences, see Table 4). The oligonucleotide on the 5′ end is known as the "up" probe and the oligonucleotide on the 3′ end is known as the "down" probe. RNA was extracted from virus-treated neurons; 0.2-10 ng of RNA was used with 0.68 µl each of the "up" and "down" probes (at 40 nM), 1 µl dNTPs (5 µM), and 1.7 µl 10× Cut Smart Buffer (1×) mixed in a total volume of 17 µl per reaction. Probes were annealed using the following protocol on the thermocycler: 90°C for 1 min, 80°C for 1 min, 70°C for 1 min, 60°C for 1 min, 50°C for 1 min, 40°C for 6 min. After annealing of DNA probes, 3 µl of a master mix with 1.25 µl Bst 2.0 DNA polymerase (0.01 U, New England Biolabs), 0.4 µl SplintR Ligase (0.5 U, New England Biolabs), and 1.35 µl ATP (10 nmol) was added per reaction and incubated for 20 min at 45°C, followed by 20 min at 80°C, then stored at 4°C. Selected DNA was then used for qPCR as previously described, where a decrease in m^{6}A means more product and therefore lower threshold cycle (C_t) values.

Formaldehyde RNA immunoprecipitation (fRIP). fRIP was performed with modified protocols from Selth et al. (2009) and Hendrickson et al. (2016). Samples were homogenized in PBS and cross-linked using 0.1% formaldehyde (methanol-free) for 5 min at room temperature. Cross-linking was quenched using 125 mM glycine. Samples were centrifuged at 8000 rpm for 2 min and then washed extensively using PBS and 1× protease inhibitor. Samples were resuspended in 1 ml lysis buffer (25 mM Tris-HCl, pH 7.5, 150 mM KCl, 5 mM EDTA, and 0.5% NP-40 with 1:1000 RNaseOUT, 1 M DTT, and 1× PIC fresh); 56 µl of each sample was reserved as the input material (i.e., did not undergo IP), and the rest was split in half (one half underwent IP with DPYSL2 antibodies and the other half with CYFIP2 antibodies; for antibody details, see Table 2); 5 µg of antibody was added to each IP and rotated at 4°C for 2 h, after which 50 µl of Dynabeads Protein G beads (Fisher Scientific) was added to the antibody-lysate mix and rotated for 1 h at 4°C to isolate protein-bound RNA from the beads. The beads were then washed with native lysis buffer and resuspended in 56 µl of ultrapure water, which was reverse-cross-linked; 33 µl of reverse-crosslinking buffer (3× PBS, 6% N-lauroyl sarcosine, 30 mM EDTA, 15 mM DTT, 1:1000 RNaseOUT, and 1× PIC) was added to all samples and incubated at 42°C for 1 h followed by 55°C for another hour to separate cross-linked RNA and protein. RNA was extracted using RNAClean XP beads (Beckman Coulter) and DNase-treated (using the Zymo DNase enzyme and buffer as per the manufacturer's protocols). RNA was eluted in 11 µl of RNase-free water and used for qRT-PCR.

Imaging analysis. Primary cortical neurons were transduced with CIRTS control and CIRTS-FTO viruses, 2 d post-plating on glass poly-D-lysine-coated coverslips. Seven days later, cells were fixed with 4% PFA for 10 min at room temperature, washed for 5 min with 100 mM

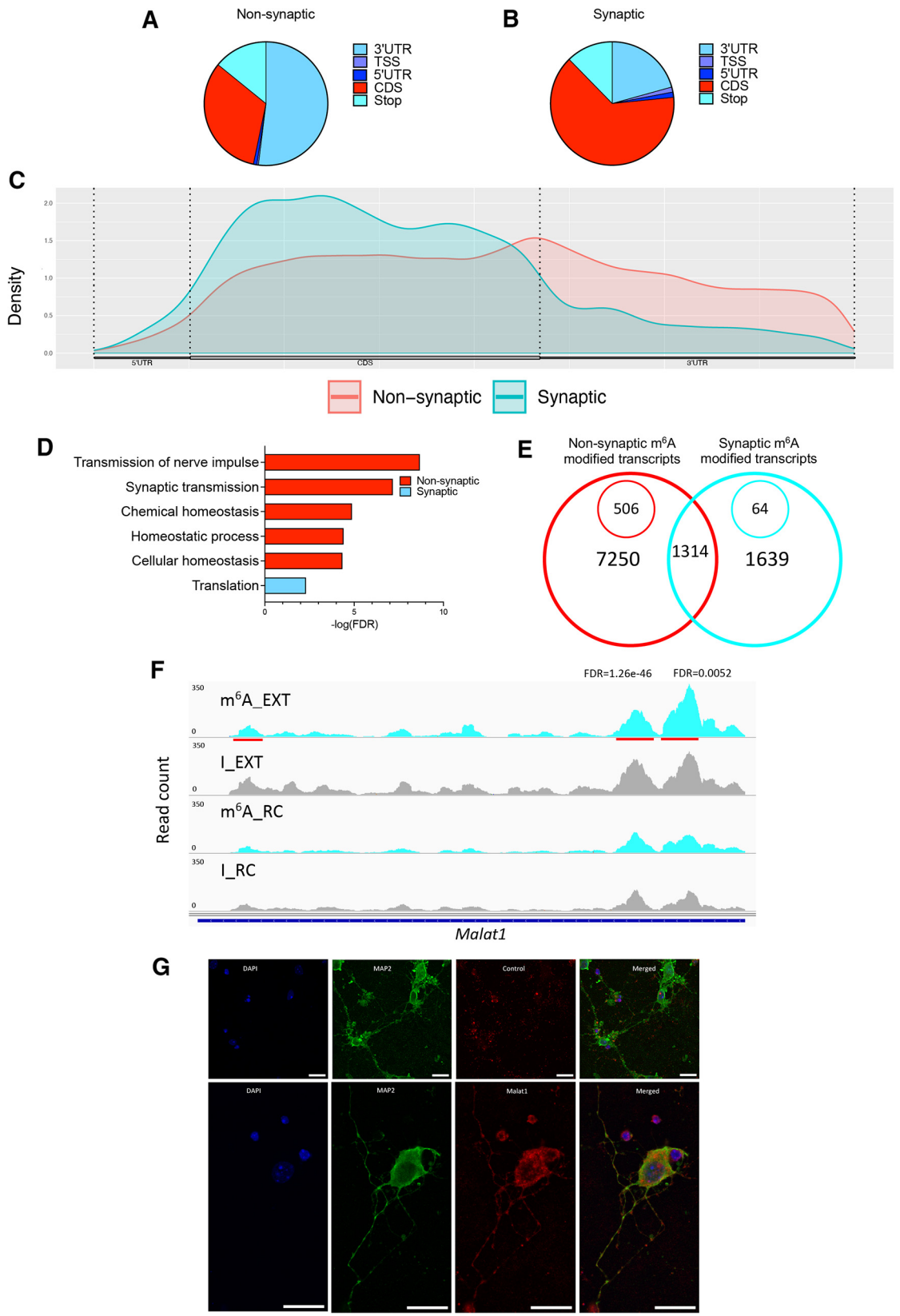

Figure 1. A distinct population of RNAs is found at the synapse after fear-extinction learning. Low-input m^{6}A-sequencing revealed the distribution of m^{6}A marks along transcripts in (***A***). Nonsynaptic and (***B***) synaptic fractions where the majority of m^{6}A marks in nonsynaptic transcripts accumulate in the 3′UTR compared with the CDS (coding sequence) in synaptic transcripts. TSS, Transcription start site; 5′UTR, 5′ untranslated region (***C***). ***D***, Biological process GO analysis terms for significantly modified transcripts in each fraction with m^{6}A-modified transcripts having different functions based on their cellular localization. ***E***, Venn diagram highlights 7250 m^{6}A-modified transcripts in the nonsynaptic fraction, 506 of which were significantly modified after EXT training compared with input controls. Similarly, 1639 synaptically localized m^{6}A-modified transcripts were identified, 64 of which were significantly modified after EXT training. mPFC nonsynaptic and synaptic lysates from RC or EXT animals; each had input and m^{6}A-enriched samples ($n = 3$, where each replicate was a pool of 4 mPFCs). Representative Integrated Genome Viewer track (***F***) showing *Malat1* (synaptic target, blue) in m^{6}A and input groups after RC or EXT, where significant peaks (false discovery rate [FDR] < 0.05) represent those with a greater number of

Table 3. CIRTS DNA sequences[a]

DNA fragment name	Sequence
FTO FL	ATGGGAATTATCAACACCCTTCAAAAATACTACTGTCGCGTCCGTGGGGGTCGTTGCGCAGTCCTGTCGTGCCTGCCTAAAGAGGAGCAGATCGGTAAATGCTCAACCCGTGGACGTA AGTGCTGTCGTCGCAAGAAAGGCGGTTCTGGAGGCTCAGGGGGGAGCGGAGGGTCCGGTGGATCAGGAGGCTCCATGGCAGTTCCCGAGACCCGCCCTAACCACACTATTTATATCAA CAACCTCAATAGCAAGATCAAGAAGGATGAGCTAAAAAAGTCCCTGTACGCCATCTTCTCCCAGTTTGGCCAGATCCTGGATATCCTGGTACCGCGGCAGCGTACCCCGAGGGGCCAGGC CTTTGTCATCTTCAAGGAGGTCAGCAGCGCCACCAACGCCCTGCGCTCCATGCAGGGTTTCCCTTTCTATGACAAACCTATGCGTATCCAGTATGCCAAGACCGACAAACGTATCCCGGC CAAGATGAAAGGCACCTTCGTGGGATCCCTTCAACTGCCTCCACTTGAAAGACTGACACTGGGCGGTAGTGGAGGAAGCGGGGGGAGCGGAGGGAGTGGTGGATCCGGCGGCTCCAAGCG CGTCCAGACCGCGGAGGAACGAGAGCGGGAAGCTAAGAAACTGAGGCTCCTTGAGGAGCTTGAAGACACTTGGCTTCCTTACCTGACCCCAAAGATGATGAGTTCTATCAGCAGTGGCA GCTGAAATACCCTAAACTGGTTTTCCGAGAGGCCGGCAGCATACCAGAGGAGCTGCATAAGGAGGTCCCCGAGGCCTTTCTCACACTGCATAAGCATGGCTGCTTGTTTCGGGACGTGGT GAGGATCCAAGGCAAAGATGTGCTCACCCCAGTGTCTCGCATCCTCATCGGGGACCCAGGCTGCACCTACAAGTACTTGAACACCAGACTCTTCACGGTGCCCTGGCCCGTGAAGGGCTG CACGGTCAAGTACACAGAGGCTGAGATCGCCGCTGCATGTCAGACCTTCCTAAAGCTCAATGACTACCTCCAGGTGGAGACCATCCAGGCCTTGGAAGAACTGGCTGTCAGAGAGAAGGC CAATGAAGACGCTGTGCCACTGTGCATGGCAGAGTTCCCCAGGGCCGGCGTGGGGCCGTCCTGCGATGATGAAGTGGACCTTAAGAGCAGAGCAGCCTACAACGTGACTTTGCTAAACTT CATGGATCCTCAGAAGATGCCCTACTTGAAAGAGGAGCCCTATTTCGGCATGGGGAAGATGGCGGTGAGCTGGCATCACGATGAGAACCTGGTGGACAGGTCAGCCGTGGCAGTGTACAG CTATAGCTGCGAAGGCTCTGAGGATGAAAGTGAGGACGAGTCCAGCTTCGAAGGCAGAGATCCTGATACTTGGCATGTTGGTTTTAAGATCTCTTGGGACATCGAGACACCAGGATTAAC AATCCCTCTTCACCAGGGAGACTGCTATTTCATGCTGGATGACCTCAATGCCACCCACCAGCACTGTGTTTTGGCTGGCTCACAGCCTCGGTTTAGTTCCACTCACCGTGTGGCAGAGTG CTCAACAGGCACCTTGGATTATATCTTAGAACGCTGTCAGTTGGCGCTGCAGAATGTCCTCAATGACTCAGACGATGGCGACGTCTCGTTGAAATCCTTTGATCCTGCAGTTTTGAAACA AGGAGAGGAAATCCATAATGAGGTGGAGTTTGAGTGGCTGAGGCAGTTCTGGTTTCAAGGCAATCGATACAAACTTTGCACCGATTGGTGGTGTGAGCCCATGACTCACCTGGAGGGGCT GTGGAAGAAGATGGAGAGCATGACAAATGCGGTGCTCCGTGAAGTTAAAAGAGAGGGGCTCCCGGTGGAACAAAGGAGTGAGATTCTGTCTGCCATCCTGGTCCCGCTCACCGTGCGCCA GAACCTGAGGAAGGAGTGGCATGCCAGGTGCCAGTCCCGAGTCGTCCGGACTTTACCAGTACAGCAGAAACCAGACTGCCGGCCATATTGGGAGAAGGATGACCCTTCCATGCCTCTGCC CTTTGACCTCACAGACGTGGTTTCCGAGCTCAGAGGCCAGCTGCTGGAAGCAAGATCCTAG
Peak 1	GAGGGCCTATTTCCCATGATTCCTTCATATTTGCATATACGATACAAGGCTGTTAGAGAGATAATTGGAATTAATTTGACTGTAAACACAAAGATATTAGTACAAAATACGTGACGTAGA AAGTAATAATTTCTTGGGTAGTTTGCAGTTTTAAAATTATGTTTTAAAATGGACTATCATATGCTTACCGTAACTTGAAAGTATTTCGATTTCTTGGCTTTATATATCTTGTGGAAAGGA CGAAACACCGGCCAGATCTGAGCCTGGGAGCTCTCTGGCCTTATT**CCAAATACTAGCCTAACCTTTTTGTTTTTT**TTTTTGGATAAGCTTGATATCGAATT
Peak 2	GAGGGCCTATTTCCCATGATTCCTTCATATTTGCATATACGATACAAGGCTGTTAGAGAGATAATTGGAATTAATTTGACTGTAAACACAAAGATATTAGTACAAAATACGTGACGTAGA AAGTAATAATTTCTTGGGTAGTTTGCAGTTTTAAAATTATGTTTTAAAATGGACTATCATATGCTTACCGTAACTTGAAAGTATTTCGATTTCTTGGCTTTATATATCTTGTGGAAAGG ACGAAACACCGGCCAGATCTGAGCCTGGGAGCTCTCTGGCCTTATT**CCTCAGTCCTTCCTAGCTTCACCAAACTGG**TTTTTGGATAAGCTTGATATCGAATT
Peak 3	GAGGGCCTATTTCCCATGATTCCTTCATATTTGCATATACGATACAAGGCTGTTAGAGAGATAATTGGAATTAATTTGACTGTAAACACAAAGATATTAGTACAAAATACGTGACGTAGA AAGTAATAATTTCTTGGGTAGTTTGCAGTTTTAAAATTATGTTTTAAAATGGACTATCATATGCTTACCGTAACTTGAAAGTATTTCGATTTCTTGGCTTTATATATCTTGTGGAAAGGA CGAAACACCGGCCAGATCTGAGCCTGGGAGCTCTCTGGCCTTATTT**ATGGTTTTAATGTTAAATTACAGGCAAGGG**TTTTTGGATAAGCTTGATATCGAATT
Control guide	GATACATCATCTCTGTATTAGGCTCCCAAC

[a]Sequences of DNA fragments cloned into CIRTS plasmids where the *Malat1* sequence is in bold. Three m^{6}A sites (or peaks) were targeted using the CIRTS plasmids; hence, three guides were designed which correspond to each site.

glycine in PBS to quench the reaction, then washed 3 times with 1× PBS, at 5 min per wash. Fixed cells were permeabilized by incubating in 0.4% Triton X-100 in 1× PBS for 15 min at room temperature and immunohistochemistry was continued as above. Neurons were imaged with a spinning disk confocal system (Yokogawa Corporation of America) using a 100× oil objective. Image acquisition was performed using SlideBook 6.0 (3I) with 0.34 μm *z* step used to collected *Z* stacks for each neuron. Each image was analyzed in Neurolucida 360 (MBF Bioscience) with dendrites traced and spines identified. Dendritic spines were identified using the following parameters: maximum height, 2.5 μm; minimum height, 0.3 μm; voxels, 10 and detector sensitivity of 85%. Spines were classified into specific morphology (filopodia, thin, stubby, and mushroom) by MBF software. Classifications, the number of spines, spine density, and measurements were exported from Neurolucida Explorer into Excel files for data analysis.

Statistical analysis. All statistical analyses were performed using Prism 9. A two-tailed unpaired Student's *t* test was used for comparison between groups in m^{6}A enriched, unmodified, and IgG control fractions, as well as CIRTS Control and *Malat1* groups. One-way or two-way ANOVA was chosen for multiple comparisons where appropriate. All *post hoc* analysis was performed using Dunnett's multiple comparison test. Error bars indicate SEM where significance was taken as $p < 0.05$.

Table 4. Oligonucleotides sequences for SELECT assay[a]

Name	Sequence
Up probe Peak 1	tagccagtaccgtagtgcgtgGGACAGAACTTTTTTGTTTTTC
Down probe Peak 1	5phos/ATCTTCTTTCTCCAAATACTAGCcagaggctgagtcgctgcat
Up probe Peak 2	tagccagtaccgtagtgcgtgAGGGCTTCGGTCAAACCACTT
Down probe Peak 2	5phos/GCTGGCTCCTCAGTCCTTCcagaggctgagtcgctgcat
Up probe Peak 3	tagccagtaccgtagtgcgtgGTTAAAAGGGGAACGGACATT
Down probe Peak 3	5phos/ATCTTAGCTATGGTTTTAATGcagaggctgagtcgctgcat

[a]Sequences of Up (oligonucleotide which anneals at the 5′ end) and Down (oligonucleotide which anneals at the 3′ end) probes for each m^{6}A site/peak targeted using CIRTS.

Results

m^{6}A-modified RNAs accumulate within the synaptic compartment following fear-extinction learning

Given that the pattern of RNA expression can differ based on cellular localization and training context, we examined the levels of synaptic m^{6}A-modified RNA following fear-extinction learning. Tissue derived from either RC or EXT-trained animals was used to isolate RNA from the synaptic compartment and subjected to low-input RNA m^{6}A-sequencing. A total of 24 libraries were sequenced, which included three biological replicates (where each replicate is a pool of four mPFCs) per group (RC Input, EXT Input, RC m^{6}A-enriched, and EXT m^{6}A-enriched) for nonsynaptic and synaptic fractions. The peak distribution along modified transcripts in the nonsynaptic fraction showed an accumulation of m^{6}A in the 3′UTR (Fig. 1*A*,*B*,*F*). In contrast, the majority of peaks along transcripts in the synaptic fraction were found in the coding sequence (CDS, Fig. 1*A*,*C*). The difference in distribution of m^{6}A marks in different compartments suggested the possibility that m^{6}A-modified RNA serves a functionally distinct role in the synapse compared with other neuronal compartments. We therefore performed a GO term analysis for

←

reads in the m^{6}A group compared with the input control after EXT. The m^{6}A sites targeted for subsequent experiments are underlined in red. For m^{6}A peaks detected, see Extended Data Figure 1-1. For the significantly modified transcripts identified using low-input m^{6}A sequencing in nonsynaptic and synaptic fractions after fear-extinction learning, see Extended Data Figure 1-2. Each line indicates an m^{6}A site, and there are multiples line of data per gene. ***G***, RNABaseScope confocal images of neurons show the trafficking of *Malat1* along dendrites in primary cortical neurons (DIV 7). Left images, DAPI labeling. Middle, GFP panels label the morphology of neurons (anti-MAP2 primary antibody) and Fast Red dye labels the RNA of interest (negative control is a probe designed against a bacterial enzyme or a probe designed against *Malat1*). Right images, DAPI, GFP, and Fast Red merged images. Scale bars, 20 μm.

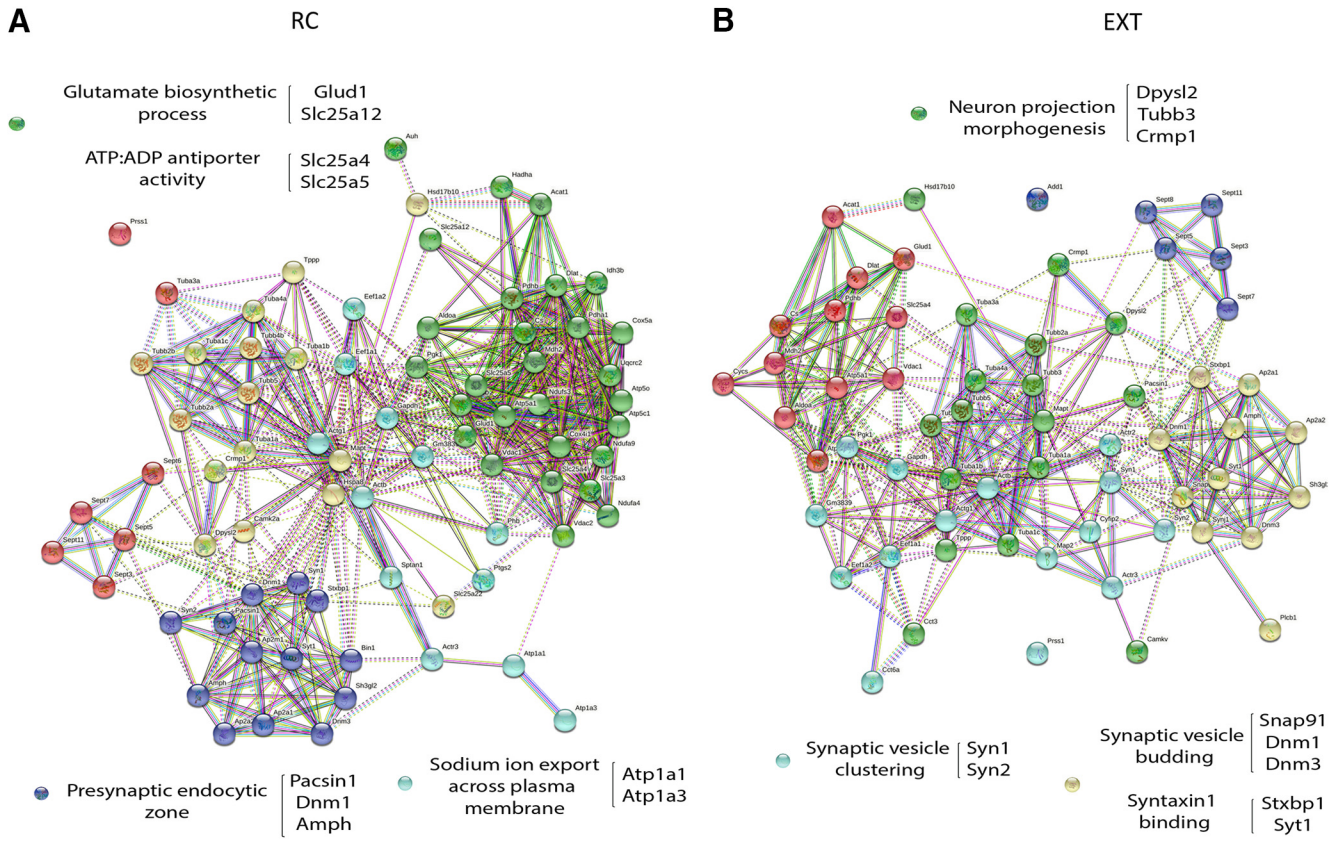

Figure 2. Novel synaptic m^{6}A readers are found in the context of fear-extinction learning. Representative functional interaction network analysis of m^{6}A-interacting proteins in (***A***) RC and (***B***) EXT groups at the synapse after extinction training. RIP-MS was performed using control and m^{6}A synthetic biotinylated oligonucleotides to pull-down proteins in mPFC synaptic lysates from RC or EXT-trained mice ($n = 3$ per group; each replicate is a pool of 4 mPFCs). For the full list of m^{6}A readers in each group identified using RIP-MS, see Extended Data Figure 2-1.

significantly modified transcripts, which revealed that the nonsynaptic m^{6}A-modified RNA was associated with cellular transmission and nerve impulse transmission, whereas the synaptic m^{6}A-modified RNA was related to translation (Fig. 1*D*).

In the nonsynaptic fraction, we identified a total of 15,716 m^{6}A peaks (Extended Data Fig. 1-1). These mapped to 7250 genes, with 506 transcripts being significantly enriched compared with input after EXT training (Fig. 1*E*; Extended Data Fig. 1-2). Many of the m^{6}A-modified transcripts, including *Camk2a* and *Grin2b* (Merkurjev et al., 2018; Shi et al., 2018) as well as *Shank1* and *Homer1* (Sala et al., 2001), are known to be functionally related to plasticity and memory. In the synaptic fraction, a total of 2126 m^{6}A peaks were identified (Extended Data Fig. 1-1), which mapped to 1639 genes. Of these, 64 were significantly enriched compared with input after EXT training (Fig. 1*A*; Extended Data Fig. 1-2). In addition to several known m^{6}A-modified RNAs, such as *Kif5a*, *Atp1a2*, and ribosomal subunits *Rpl13*, *Rpl21*, *Rpl23a*, and *Rpl26*, which have been previously identified at the synapse under baseline conditions (Merkurjev et al., 2018) we discovered novel, extinction earning-related m^{6}A-modified transcripts, including *Trim2*, *Calr*, *Man1a2*, *Malat1*, and *Ncam2*. Previously thought to be selectively expressed in nuclear speckles and associated with the alternative splicing of *Nlgn1* and *SynCam1* (Colasse et al., 2010), *Malat1* has recently been shown to be trafficked to the synapse (Alon et al., 2021), suggesting that its local activity may contribute to neural growth and synaptogenesis (Briggs et al., 2015; X. Zhang et al., 2017).

To validate our finding that m^{6}A-modified *Malat1* accumulates at the synapse (Fig. 1*F*), we used RNA BaseScope, which revealed that *Malat1* is present in dendritic compartments and trafficked to the synapse in primary cortical neuron (Fig. 1*G*). These findings add to the growing appreciation of the multifunctional capacity for lncRNAs in the adult brain.

Novel synaptic m^{6}A readers associated with fear-extinction learning

Previous studies have identified m^{6}A-modified RBPs, including YTHDF2/3, YTHDC1, ELAVL1, FMRP, and IGF2BP1 (Dominissini et al., 2012; Huang et al., 2018; Edens et al., 2019), some of which are expressed at the synapse (Merkurjev et al., 2018). However, no study has determined whether there are learning-specific m^{6}A-modified RNA-interacting RBPs in the synaptic compartment. Using a synthetic biotinylated control and m^{6}A-modified oligonucleotides, we sought to identify synaptic m^{6}A readers that are specific to fear-extinction learning. C57/BL6 mice were trained using a standard cued fear-conditioning task followed by either novel context exposure (RC) or EXT training. Immediately after training, the mPFC was extracted for the isolation of synaptosomes followed by m^{6}A-modified RIP mass spectrometry (m^{6}A-RIP-MS). In the synaptic fraction derived from RC-trained animals, we identified 77 proteins that interacted with m^{6}A-modified RNA (Extended Data Fig. 2-1), with many of these proteins being associated with mitochondrial function (Fig. 2*A*). In comparison, within the synapse-enriched fraction of EXT-trained animals, 62 proteins were found to interact with m^{6}A-modified RNA (Fig. 2*B*). These proteins were functionally distinct from those in the RC group, and included proteins involved in synaptic vesicle clustering (SYN1, SYN2) and budding (SNAP91,

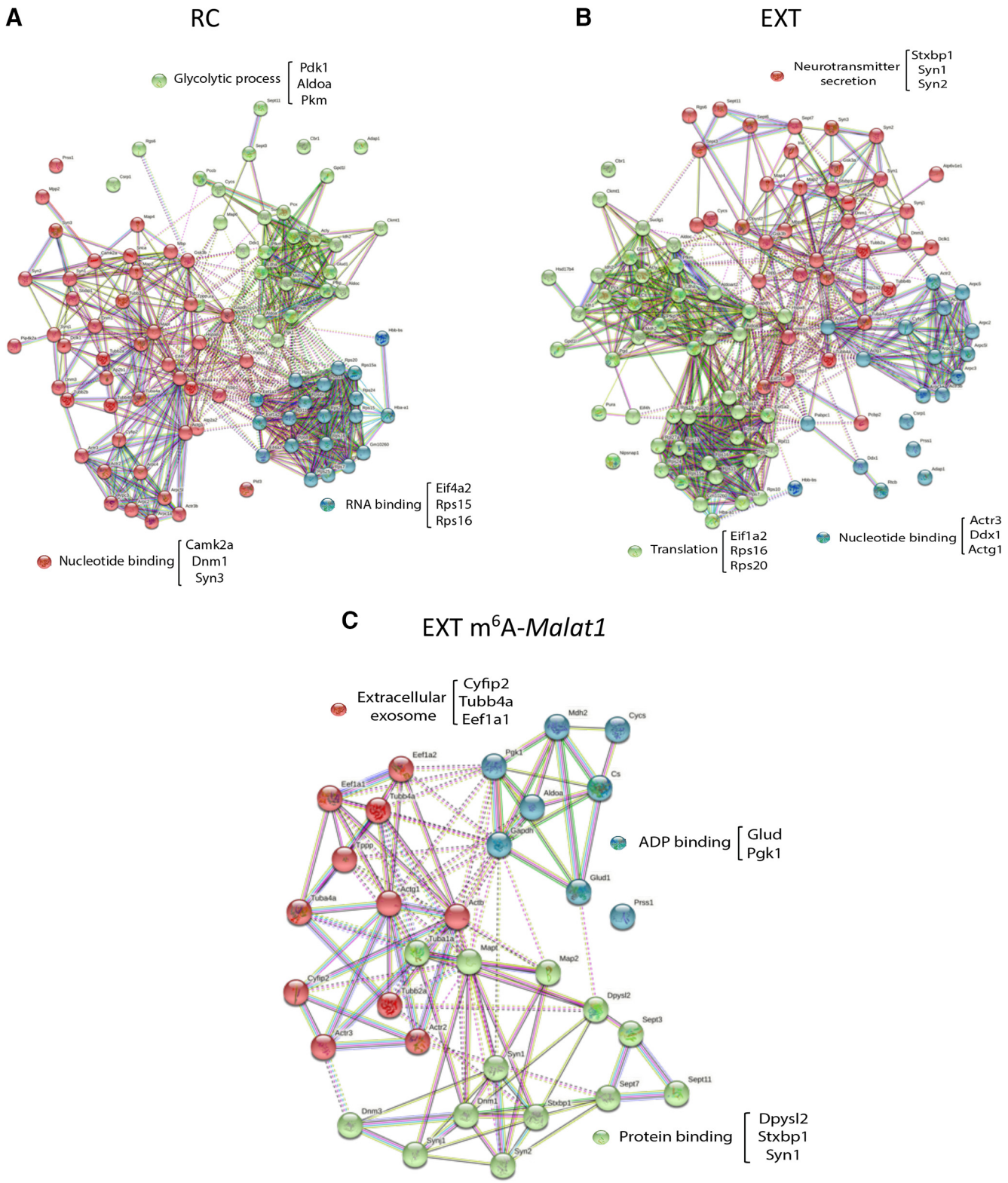

Figure 3. *Malat1* interacts with m^{6}A readers at the synapse after fear-extinction learning. Representative functional interaction network analysis of *Malat1* interaction proteins in (***A***) RC and (***B***) EXT groups, and (***C***) m^{6}A readers which also interact with *Malat1* at the synapse after EXT ($n = 3$ per group; each replicate is a pool of 4 mPFCs). RIP-MS was performed using synthetic biotinylated oligonucleotides complementary to *Malat1* (designed at chr19: 5797504-5797533) to pull-down proteins bound to endogenous *Malat1* in mPFC synaptic lysates from EXT-trained mice. For the full list of m^{6}A readers in each group identified using RIP-MS, see Extended Data Figure 3-1.

DNM1, DNM3), neuron projection morphogenesis (DPYSL2, TUBB3, CRMP1), and translation elongation activity (EEF1A1, EEF1A2). Overall, we identified 12 synapse-specific m^{6}A readers that were unique to EXT learning, including proteins that are associated with synaptic plasticity (CYFIP2, ADD1) (Matsuoka et al., 1998; Marsden et al., 2018), synaptic vesicle formation (SEPT8) (Ito et al., 2009), or calmodulin binding (CAMKV) (Godbout et al., 1994).

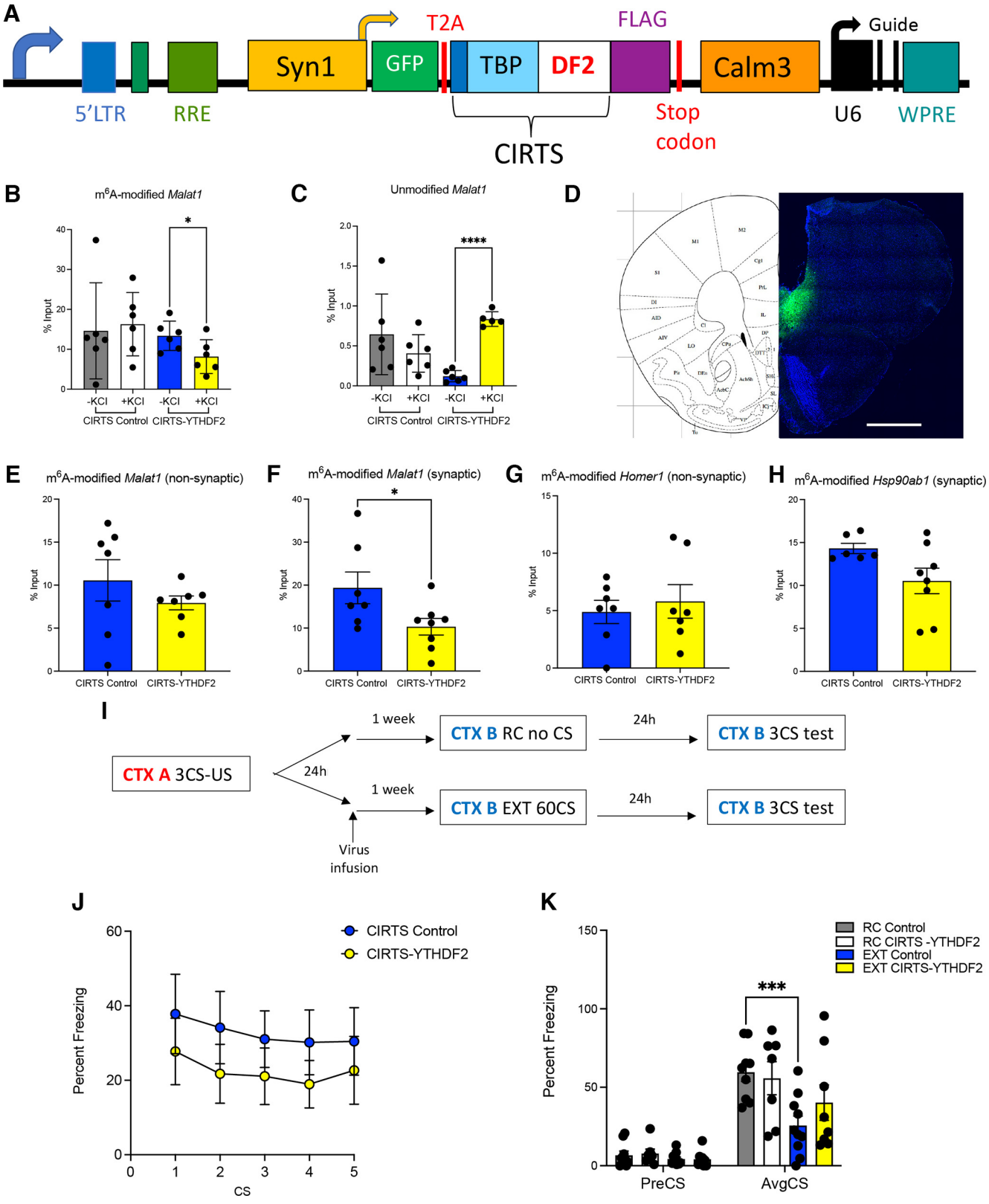

Figure 4. Targeted degradation of m^{6}A-modified Malat1 at the synapse impairs fear-extinction memory. ***A***, Schematic of CIRTS-YTHDF2 construct used for targeted degradation of *Malat1*. ***B***, ***C***, *In vitro* validation of CIRTS-YTHDF2 constructs indicates a decrease in m^{6}A-modified *Malat1*, which was accompanied by an increase in unmodified *Malat1* expression. ***B***, m^{6}A-modified *Malat1* ($n = 6$ in all groups; two-tailed, unpaired Student's *t* test between CIRTS-YTHDF2 -KCl vs CIRTS-YTHDF2 +KCl, $t = 2.285$, df = 10, $p = 0.0454$) and (***C***) unmodified *Malat1* ($n = 6$ in all groups, except $n = 5$ in the CIRTS-YTHDF2 +KCl group; two-tailed, unpaired Student's *t* test, $t = 14.70$, df = 9, $p < 0.0001$) expression compared with input controls in control (CIRTS construct with control gRNA) or CIRTS-YTHDF2-transduced neurons with or without KCl treatment. ***D***, Representative image of viral infusion of CIRTS virus in the ILPFC. Scale bar, 1000 μ ***E***, ***F***, *In vivo* validation of CIRTS-YTHDF2 virus in synaptic and nonsynaptic lysates isolated from mPFCs of EXT-trained mice. There were no significant differences in m^{6}A-modified *Malat1* expression levels in the (***E***) nonsynaptic compartment ($n = 7$ in the CIRTS control group and $n = 8$ in the CIRTS-YTHDF2 group, unpaired Student's *t* test between CIRTS control vs CIRTS-YTHDF2, $t = 0.1450$, df = 13, $p = 0.8870$). However, a significant decrease in m^{6}A-modified *Malat1* expression levels was observed (***F***) in the synaptic compartment ($n = 7$ in the CIRTS control group

Malat1 interacts with m^{6}A readers in the synaptic compartment following fear-extinction learning

Given that m^{6}A-modified *Malat1* localizes to the synapse in response to fear-extinction learning, we next investigated whether there are m^{6}A readers that are specific to m^{6}A-modified *Malat1* at the synapse. In the RC group, 92 proteins uniquely bound to the *Malat1* oligonucleotides compared with 100 proteins in the EXT group (Extended Data Fig. 3-1). The proteins that interacted with *Malat1* in the RC group were associated with RNA binding (EIF4A2, RPS15, RPS16), nucleotide binding (CNM1, SYN3), and glycolytic processes (ALDOA, PDK) (Fig. 3*A*). In comparison, EXT-dependent *Malat1* RBPs were associated with nucleotide binding (DDX1, ACTG1), as well as neurotransmitter secretion (STXBP1, SYN1, SYN2) and translation (RPS16, RPS20, EIF1A2). These data suggest that the proteins that bind to *Malat1* in the synaptic compartment also differ based on the learning context.

To determine which of the 100 EXT *Malat1* RBPs are also m^{6}A readers, we compared them with the 62 m^{6}A proteins identified at the synapse after EXT training. Thirty-two overlapping proteins were found to recognize both m^{6}A and *Malat1* at the synapse. These proteins were associated with ADP binding (GLUD, PGK), extracellular exosomes (CYFIP2, TUBB4A, EEF1A1), and protein binding (DPYSL2, STXBP1, SYN1) (Fig. 3*C*).

Targeted degradation of m^{6}A-*Malat1* at the synapse leads to impaired fear-extinction memory

To explore whether m^{6}A-modified *Malat1* and its protein interactions at the synapse are required for fear-extinction memory, we used the CIRTS plasmid to trigger the degradation m^{6}A-modified *Malat1* by targeting it with the m^{6}A reader YTHDF2 (Fig. 4*A*). The CIRTS technique can be used to deliver specific effector proteins to an RNA of interest. It consists of four components: an RNA hairpin-binding protein that selectively binds to a specific RNA structure, a gRNA with sequence complementarity to the RNA of interest, a charged protein to stabilize and protect the gRNA, and an effector protein that acts on the RNA of interest. The constructs were initially validated in primary cortical neurons (Fig. 4*B*,*C*) followed by *in vivo* tests to determine whether the selective degradation of m^{6}A-*Malat1* at the synapse (Fig. 4*E*–*H*), influences fear-extinction memory.

Targeted synaptic degradation of m^{6}A-modified *Malat1* before EXT training had no effect on within-session performance (Fig. 4*J*). However, when testing for memory, those mice with the control virus that underwent EXT training showed significantly decreased freezing scores (Fig. 4*K*). A similar decrease in freezing scores was not observed in the EXT-trained mice infused with the CIRTS-YTHDF2 virus with guides against *Malat1*, thereby revealing impaired consolidation of fear-extinction memory. These data demonstrate that m^{6}A-modified *Malat1* is critical for fear-extinction memory, and further imply a role for the interaction between m^{6}A-modified *Malat1* and specific RBPs in this process.

Targeted removal of m^{6}A on *Malat1* at the synapse leads to impaired fear-extinction memory

To further explore whether the m^{6}A modifications along *Malat1* are required for fear-extinction memory, we used a CIRTS-FTO plasmid (Fig. 5*A*) *in vivo*. Targeted demethylation of *Malat1* via CIRTS-FTO was validated using immunohistochemistry to visualize the localization of the construct (Fig. 5*B*), and a SELECT methylation assay was used to confirm demethylation at chosen sites (Fig. 5*C*–*E*). Successful demethylation was evidenced by a decrease in qPCR C_t values in neurons transduced with CIRTS-FTO virus with *Malat1* guides after KCl stimulation. This decrease in C_t values indicated an increase in selected DNA as a result of lower m^{6}A levels along *Malat1*.

Like the CIRTS-YTHDF2-mediated degradation of m^{6}A-modified *Malat1*, targeted demethylation of specific sites along *Malat1* before EXT training had no effect on within-session performance (Fig. 5*G*). However, when testing for extinction memory, the mice treated with the control virus that underwent EXT training showed significantly decreased freezing scores (Fig. 5*H*). This effect was not observed in the EXT-trained mice infused with the CIRTS-FTO virus with guides against *Malat1*, suggesting an impairment in fear-extinction memory.

Malat1 interacts with DPYSL2 in an m^{6}A-dependent manner

To determine whether the impairments in fear-extinction memory observed above are because of a lack of interactions between *Malat1* and m^{6}A reader proteins on demethylation/degradation of *Malat1*, we used CIRTS-FTO in primary neurons. Following targeted demethylation, fRIP-qPCR (Fig. 6*A*) was performed with primers designed against the targeted m^{6}A sites. CYFIP2 and DPYSL2 antibodies were used to determine the changes in expression of *Malat1* binding to these proteins after demethylation. The m^{6}A readers CYFIP2 and DPYSL2 were chosen as proteins of interest as they showed a strong interaction with *Malat1* at the synapse (Fig. 3*C*). They also belong to the WAVE complex and serve to influence actin dynamics at the synapse (Kawano et al., 2005; Kim et al., 2006; Takenawa and Suetsugu, 2007; Z. Chen et al., 2010), which is critical for memory consolidation (Soderling et al., 2007). Based on fRIP-qPCR, we found that the levels of *Malat1* bound to CYFIP2 remained unchanged across all m^{6}A sites (Fig. 6*E*–*G*). However, the levels of *Malat1* bound to DPYSL2 increased without KCl treatment (likely a result of active demethylation already occurring at the synapse) but returned to baseline on KCl stimulation following demethylation at Site 1 (Fig. 6*B*) but not Sites 2 or 3 (Fig. 6*C*,*D*). These data

←

and $n = 8$ in the CIRTS-YTHDF2 group, unpaired Student's t test between CIRTS control vs CIRTS-YTHDF2, $t = 2.247$, df = 13, $p = 0.0426$) compared with input controls in CIRTS control or CIRTS-YTHDF2-infused animals. ***G***, ***H***, No off-target effects of the CIRTS-YTHDF2 construct were detected using qRT-PCR. ***G***, There were no significant differences in m^{6}A-modified *Homer1* expression levels in the nonsynaptic fraction ($n = 7$ per group, unpaired Student's t test between CIRTS control vs CIRTS-YTHDF2, $t = 0.5175$, df = 12, $p = 0.6142$) or (***H***) m^{6}A-modified *Hsp90ab1* expression levels in the synaptic fraction ($n = 5$ in the CIRTS control group and $n = 8$ in the CIRTS-YTHDF2 group, unpaired Student's t test between CIRTS control vs CIRTS-YTHDF2, $t = 1.723$, df = 11, $p = 0.1128$), indicating that the effects of CIRTS-YTHDF2 are specific to *Malat1* at the synapse. *Homer1* and *Hsp90ab1* were chosen as candidates in the nonsynaptic and synaptic fractions, respectively, as they were found to be significantly modified after EXT-learning using m^{6}A sequencing. ***I***, Schematic of the behavioral protocol used to test lentiviral-mediated degradation of m^{6}A-modified *Malat1* in the ILPFC on fear-extinction memory. CTX, Context; CS, conditioned stimulus (i.e., tone); US, unconditioned stimulus (i.e., foot shock). ***J***, There was no effect of CIRTS-YTHDF2 virus infusion in the ILPFC on performance during within session extinction training ($n = 10$ in the CIRTS control group and $n = 8$ in the CIRTS-YTDF2 group, two-way ANOVA, $F_{(4,64)} = 0.2246$, $p = 0.9237$; Bonferroni's *post hoc* test, all sections are $p > 0.9999$). ***K***, However, animals treated with control virus that were fear conditioned and exposed to the novel context (RC Control, $n = 9$) had significantly higher freezing scores than control animals that were extinction trained (EXT control, $n = 10$, two-way repeated-measures ANOVA, $F_{(3,30)} = 3.608$, $p = 0.0245$; Dunnett's *post hoc* test RC control vs EXT control, $p = 0.0003$) but not the RC CIRTS-YTHDF2 animals ($n = 7$). This effect was blocked in animals that were treated with CIRTS-YTHDF2 virus and extinction trained (EXT CIRTS-YTHDF2, $n = 8$, two-way repeated-measures ANOVA, $F_{(3,30)} = 3.608$; Dunnett's *post hoc* test, RC control vs EXT CIRTS-YTHDF2, $p = 0.0735$). Data are plotted as mean values. Error bars indicate SEM. $^*p < 0.05$. $^{***}p < 0.001$. $^{****}p < 0.0001$.

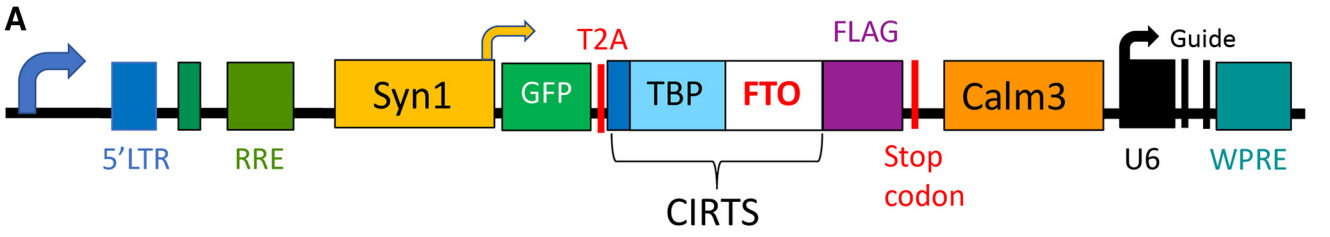

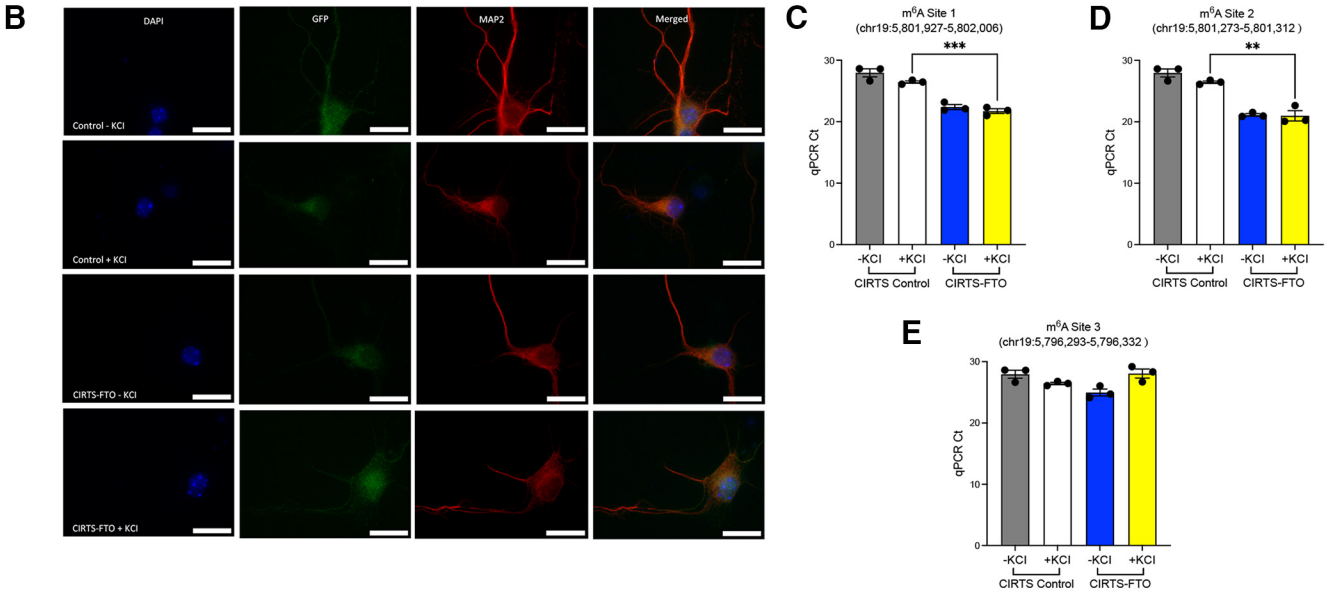

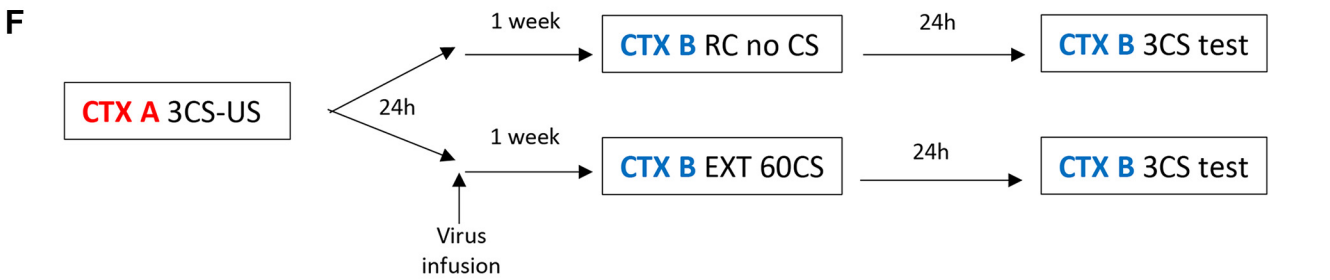

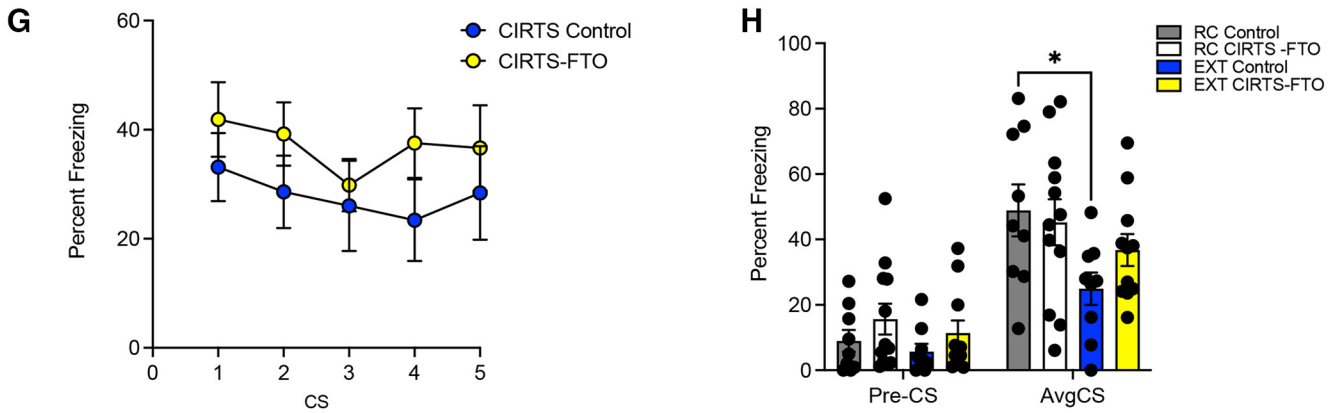

Figure 5. Targeted demethylation of *Malat1* at the synapse impairs fear-extinction memory. ***A***, Schematic of CIRTS-FTO construct used for targeted degradation of *Malat1*. ***B***, Images of dendritic processes of DIV10 primary cortical neurons expressing CIRTS control or CIRTS-FTO viruses with or without KCl treatment (20 mM, 4 h). Left images, DAPI labeling. Middle panels, Anti-GFP staining labels the location of the CIRTS construct and anti-MAP2 labeling of the morphology of neurons. Right images, MAP2 and GFP merged images. Scale bars, 20 µm. ***C–E***, Bar plots of the C_t of qPCR showing SELECT assay results detecting m^{6}A levels in *Malat1* after targeting with different gRNAs at three different m^{6}A sites: chr19: 5801927-5802006 (Site 1), chr19: 5801273-5801312 (Site 2), and chr19: 5796293-5796332 (Site 3). CIRTS-FTO decreased m^{6}A at m^{6}A Site 1 ($n = 3$ per group; two-tailed, unpaired Student's t test, $t = 10.91$, df $= 4$, $p = 0.0004$) and m^{6}A Site 2 ($n = 3$ per group; two-tailed, unpaired Student's t test, $t = 6.394$, df $= 4$, $p = 0.0031$) as indicated by the significant decrease in qPCR C_t (i.e., more product because of the lack of m^{6}A sites which no longer inhibit DNA polymerase elongation and nick ligation), compared with CIRTS control constructs in primary neurons treated with KCl. This decrease in qPCR C_t was not observed at m^{6}A Site 3 ($n = 3$ per group; two-tailed, unpaired Student's t test, $t = 2.149$, df $= 4$, $p = 0.0981$). ***F***, Schematic of protocol used to test the effect of lentiviral-meditated demethylation of m^{6}A-modified *Malat1* in the ILPFC of male C57BL/6 mice. CTX, Context; CS, conditioned stimulus (i.e., tone); US, unconditioned stimulus (i.e., foot shock). ***G***, There was no effect of

suggest that the interaction between *Malat1* and DPYSL2 is m^{6}A-dependent at specific m^{6}A sites.

Targeted demethylation of *Malat1* at the synapse leads to a reduction in the total number of dendritic spines

DPYSL2 has been implicated in the formation and maturation of dendritic spines (J. Zhang et al., 2018). Therefore, to determine the physiological effects of changes in binding of *Malat1* to DPYSL2 on demethylation, we used CIRTS-FTO in primary neurons followed by 3D reconstruction of imaged neurons to determine the effect of targeted *Malat1* demethylation on dendritic spine formation (Fig. 7*A*). We found that there was a decrease in the total number of spines after KCl stimulation in neurons treated with CIRTS-FTO targeting *Malat1* (Fig. 7*B*). However, there were no effects on the average density of spines or the percentage of thin, stubby, and mushroom spines across the neuron following *Malat1* demethylation (Fig. 7*C–F*). These results suggest that a reduced interaction between *Malat1* and DPYSL2 leads to an overall reduction in the number of dendritic spines, but not the distribution or morphology of spines across the neuron, which would then contribute to the impairment in the consolidation of fear-extinction memory. We therefore conclude that the m^{6}A-modified *Malat1*-DPYSL2 interaction is generally involved in the formation of dendritic spines.

Discussion

In this study, we found that a unique population of synapse-enriched m^{6}A-modified RNAs accumulate in response to fear-extinction learning and identified 12 extinction-learning-specific m^{6}A readers at the synapse. Fear extinction drives the expression of the m^{6}A-modified lncRNA *Malat1* at the synapse and promotes its interaction with the novel m^{6}A readers CYFIP2 and DPYSL2, both of which are critically involved in memory formation via actin polymerization at synapses and axonal growth (Y. Zhang et al., 2019; Hou, 2020). Upon targeted removal of the m^{6}A mark on *Malat1* and a degradation of m^{6}A-modified *Malat1* at the synapse, specific RNA-protein interactions can no longer occur and fear extinction memory is impaired because of a reduction in dendritic spine formation, therefore indicating a direct role for m^{6}A-modified *Malat1* in the consolidation of fear-extinction memory.

Many of the m^{6}A-modified RNAs detected at the synapse in previous studies, such as *Homer1*, *Shank1*, and *Camk2a*, were not identified after EXT learning but were instead detected in the nonsynaptic fraction. This is likely because of the time point and context at which mPFC tissue was collected. The initial study by Merkurjev et al. (2018), which identified m^{6}A-modified RNAs at the synapse, was performed using whole mouse forebrains from animals that had not undergone any behavioral training. In contrast, we conducted m^{6}A sequencing on synaptic compartments from mPFC lysates isolated immediately after fear-extinction training. As context is critical for the study of RNA modifications, these differences in brain regions (i.e., forebrain vs mPFC) and tissue collection time point (immediately after EXT training vs no training) likely account for the differences in m^{6}A-modified RNA detected in our work compared with previously published studies. However, as previously reported, the majority of RNA detected in the nonsynaptic fraction contained m^{6}A peaks in the 3′UTR (Ke et al., 2015), whereas m^{6}A peaks were more likely to occur in the CDS of RNAs detected in the synaptic fraction. The variation in the distribution of m^{6}A peaks among transcripts suggests that the functional role of m^{6}A-modified RNA depends on RNA localization. This is supported by the finding that nonsynaptic transcripts were associated with cellular transmission. In contrast, m^{6}A-modified synaptic transcripts were associated with translation, which confirms previous observations regarding the presence of m^{6}A in the CDS (Mao et al., 2019). The functional relevance of m^{6}A may therefore be dictated by the interaction between m^{6}A-modified RNA and unique reader proteins specific to each subcellular compartment.

One of the most interesting synapse-enriched m^{6}A-modified targets identified was *Malat1*, which was originally discovered in cancer cells but has also been found to be abundant in neurons (Bernard et al., 2010). *Malat1* has previously been demonstrated to be m^{6}A-modified (Dominissini et al., 2012; Meyer et al., 2012; N. Liu et al., 2013; Coker et al., 2019). This epitranscriptomic mark changes the secondary structure of *Malat1* such that proteins, including HNRNPG and HNRNPC, which are involved in splicing, can bind to it (N. Liu et al., 2015, 2017; K. I. Zhou et al., 2019; He et al., 2020). Interestingly, *Malat1* is enriched in nuclear speckles where it recruits splicing factors to genes, such as *Ngln1* and *SynCam1*. These genes are involved in synapse formation and maintenance, thereby enabling an indirect influence of *Malat1* on the synaptic density of hippocampal neurons (Bernard et al., 2010). *Malat1* has also recently been reported to be expressed in the synapse (Alon et al., 2021), although its functional relevance in the context of learning was not determined.

We have revealed a significant number of novel m^{6}A readers in the synaptic compartment after fear-extinction learning. These RBPs, which are a combination of indirect and direct m^{6}A RBPs, include the endocytosis-related protein SNAP91 (Kroll et al., 2020), CAMKV and SEPTIN8, which are important for vesicle formation (Godbout et al., 1994; Ito et al., 2009), and CYFIP2, which is necessary for synapse formation (Marsden et al., 2018). Interestingly, all are associated with memory consolidation, suggesting that m^{6}A facilitates the formation of memory through direct effects on proteins that are involved in various aspects of synaptic plasticity.

Beyond HNRNPG and HNRNPC, we found that *Malat1* interacts with numerous other m^{6}A reader proteins at the synapse in the context of fear-extinction learning. Specifically, we validated CYFIP2 and DPYSL2 binding to m^{6}A-modified *Malat1*, although only the interaction with DPYSL2 was found to be m^{6}A-dependent. CYFIP2 protein expression at the synapse contributes to actin polymerization (Pathania et al., 2014) and, therefore, synaptic plasticity through changes in spine morphology (Y. Zhang et al., 2019). Furthermore, reduced *Cyfip2* levels impair spine maturation in CA1 pyramidal neurons and prevent the retention of spatial memory (Davenport et al., 2019). DPYSL2 has also been detected in dendritic spines (Makihara et al., 2016), where post-translation modifications (phosphorylation and SUMOylation) can promote the formation and maturation of dendritic spines

←

CIRTS-FTO virus infusion in the ILPFC on performance during within session extinction training (two-way ANOVA, $F_{(4,72)} = 0.7245$, $p = 0.5781$; Bonferroni's *post hoc* test, all sections are $p > 0.9999$). ***H***, However, animals that were treated with control virus, fear-conditioned, and exposed to novel context (RC control, $n = 9$) had significantly higher freezing scores than control animals that were extinction trained (EXT control, $n = 9$, two-way repeated-measures ANOVA, $F_{(3,74)} = 1.199$, $p = 0.0307$; Dunnett's *post hoc* test, RC control vs EXT control, $p = 0.0101$) but not RC CIRTS-FTO animals ($n = 12$). This effect was blocked in animals that were treated with CIRTS-FTO virus and extinction trained (EXT CIRTS-FTO, $n = 11$, two-way repeated-measures ANOVA, $F_{(3,74)} = 1.199$; Dunnett's *post hoc* test, RC control vs EXT CIRTS-FTO, $p = 0.2604$). Data are plotted as mean values. Error bars indicate SEM. $^*p < 0.05$.

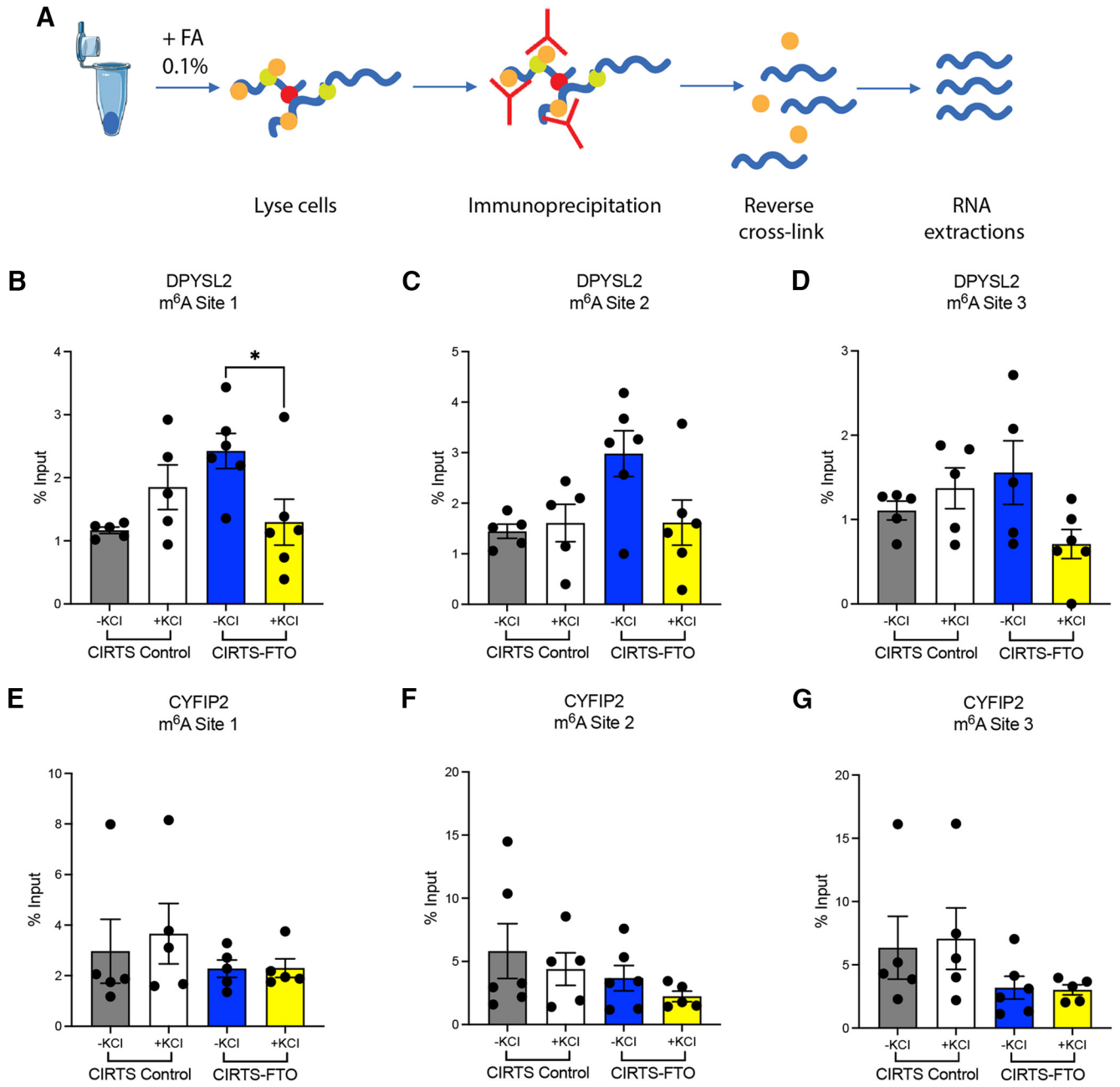

Figure 6. Site-directed demethylation and fRIP-qPCR reveal that select m^{6}A-Malat1 readers are m^{6}A-dependent. ***A***, Schematic of fRIP used to isolate RNA bound to proteins of interest. *Malat1* expression levels that bind to (***B–D***) DPYSL2 and (***E–G***) CYFIP2 at CIRTS-targeted m^{6}A sites in neurons (with or without KCl treatment) transduced with CIRTS control virus or CIRTS-FTO viruses with *Malat1* guides. The interaction between *Malat1* and DPYSL2 (***B***) is m^{6}A-dependent at Site 1 (chr19:5801927-5802006) as, following demethylation, levels of *Malat1* bound to DPYSL2 returned to baseline on KCl stimulation ($n = 5$ in the CIRTS control -KCl and CIRTS control +KCl and $n = 6$ in the CIRTS-FTO -KCl and CIRTS-FTO +KCl group; two-tailed, unpaired Student's *t* test, $t = 2.465$, df = 10, $p = 0.0334$). However, the levels of *Malat1* bound to DPYSL2 did not return back to baseline on KCl stimulation at (***C***) Site 2 (chr19:5801273-5801312; $n = 5$ in the CIRTS control -KCl and CIRTS control +KCl groups and $n = 6$ in the CIRTS-FTO -KCl and CIRTS-FTO +KCl groups; two-tailed, unpaired Student's *t* test, $t = 2.141$, df = 10, $p = 0.0579$) or (***D***) Site 3 (chr19:5796293-5796332; $n = 5$ in the CIRTS control -KCl, CIRTS control +KCl and CIRTS-FTO -KCl groups and $n = 6$ in the CIRTS-FTO +KCl group; two-tailed, unpaired Student's *t* test, $t = 2.175$; df = 9, $p = 0.0577$). There were no changes in the levels of *Malat1* binding to CYFIP2 at Site 1 (***E***) ($n = 5$ in all groups; two-tailed, unpaired Student's *t* test, $t = 0.04507$, df = 8, 0.9652), Site 2 (***F***) ($n = 6$ in the CIRTS Control -KCl and CIRTS-FTO -KCl groups and $n = 5$ in the CIRTS Control +KCl and CIRTS-FTO +KCl groups; two-tailed, unpaired Student's *t* test, $t = 1.232$, df = 9, $p = 0.2491$), or Site 3 (***G***) ($n = 5$ in the CIRTS Control -KCl, CIRTS Control +KCl and CIRTS-FTO +KCl groups and $n = 6$ in the CIRTS-FTO -KCl group; two-tailed, unpaired Student's *t* test, $t = 0.1649$, df = 9; $p = 0.8726$). Expression is calculated compared with input controls in each group. Data are plotted as mean values. Error bars indicate SEM. *$p < 0.05$.

(J. Zhang et al., 2018). DPYSL2 is also associated with axonal growth, neurotransmitter release, and synaptic physiology (Hou, 2020). Importantly, DPYSL2 conditional KO mice exhibit impaired hippocampal-dependent learning and memory impairments in the Y-maze, fear-conditioning, and the Morris water maze (H. Zhang et al., 2016).

Both CYFIP2 and DPYSL2 are associated with the WAVE regulatory complex (WRC), which is composed of five components: CYFIP1 and/or CYFIP2, NAP1 or HEM2 or KETTE, ABI2, HSPC300 or BRICK1, and WAVE1 or SCAR (B. Chen et al., 2014). Loss of function of the WRC *in vivo* or in cultured neurons results in a decrease in mature dendritic spines (Kim et

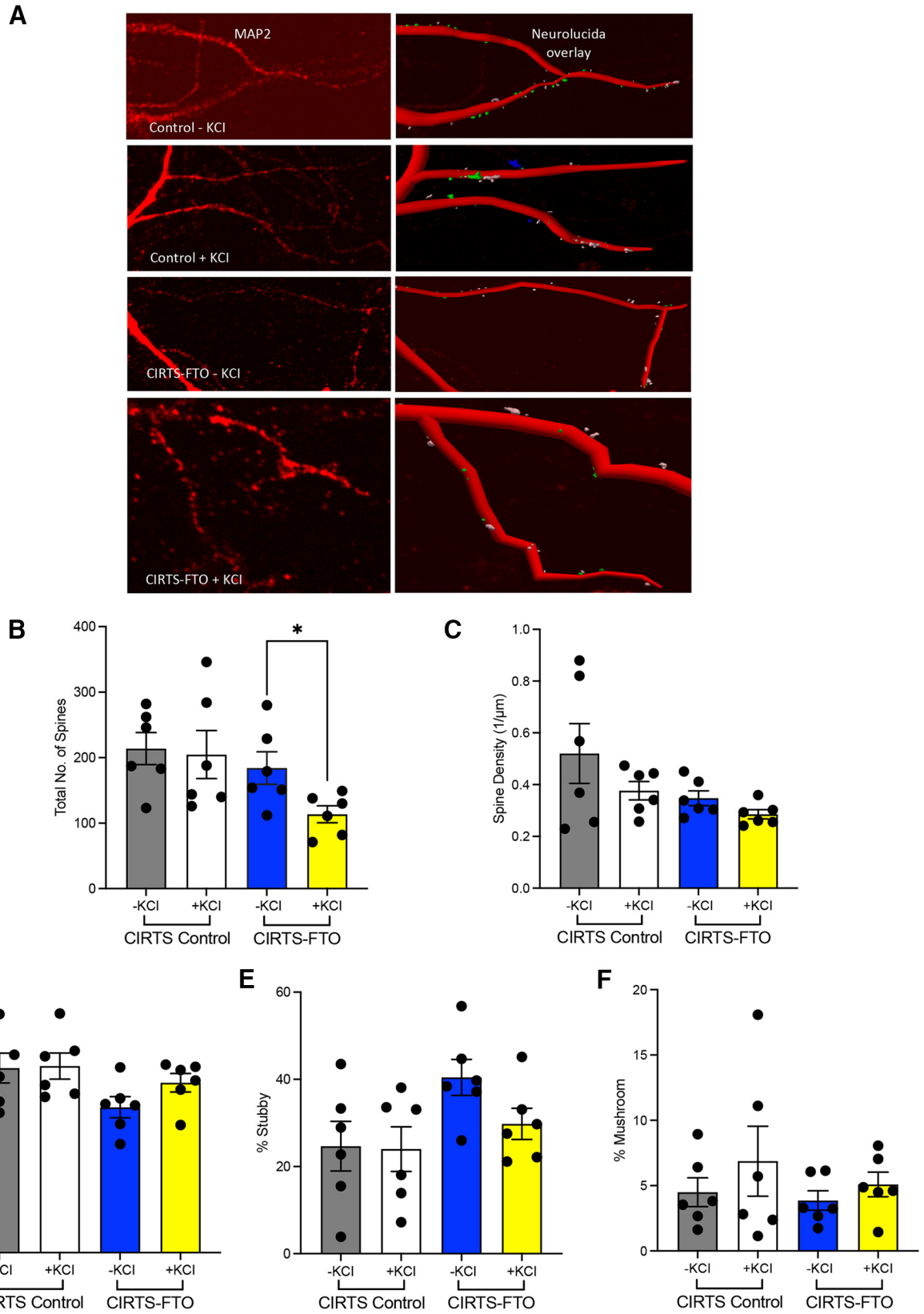

Figure 7. Site-directed demethylation of *Malat1* results in a reduction in the total number of dendritic spines. ***A***, Representative images showing MAP2 immunostaining of primary cortical neurons treated with CIRTS control or CIRTS-FTO constructs with *Malat1* guide RNAs. Right images, 3D rendering of spines detected using Neurolucida360 merged with the immunofluorescence signal. ***B***, There was a reduction in the total number of spines in neurons transduced with the CIRTS-FTO virus with *Malat1* guide RNAs and stimulated with KCl ($n = 6$ in all groups; two-tailed, unpaired Student's t test, $t = 2.532$, df $= 10$, $p = 0.0298$). However, there were no differences between groups in (***C***), overall density ($n = 6$ in all groups; two-tailed, unpaired Student's t test, $t = 1.854$, df $= 10$, $p = 0.0934$) or percentage of (***D***) thin (indicated in pink; $n = 6$ in all groups; two-tailed, unpaired Student's t test, $t = 1.744$, df $= 10$, $p = 0.1117$), (***E***) stubby (in green; $n = 6$ in all groups; two-tailed, unpaired Student's t test, $t = 1.953$, df $= 10$, $p = 0.0793$), or (***F***) mushroom (in blue; $n = 6$ in all groups; two-tailed, unpaired Student's t test, $t = 1.021$, df $= 10$, $p = 0.3314$) spines. Data are plotted as mean values. Error bars indicate SEM. *$p < 0.05$.

al., 2006). Electrophysiological recordings from hippocampal slices of WAVE1 null mice have also been shown to exhibit altered synaptic plasticity, and mutant WAVE1 mice show impaired hippocampal-dependent spatial memory (Soderling et al., 2007).

The CYFIP family of proteins and DPYSL2 serve different roles in the function of the WRC. CYFIP is a key regulator of neuronal actin dynamics in the WRC, by regulating mRNA translation and actin polymerization (De Rubeis et al., 2013; Y. Zhang et al., 2019). However, DPYSL2 is involved in the kinesin-1-dependent transport of the WAVE1 complex. Upon DPYSL2 knockdown, axonal growth is inhibited for which WAVE1 is required (Yoshimura et al., 2005). Furthermore, knockdown of DPYSL2 and kinesin1 results in the delocalization of the WAVE1 complex from the growth cones of axons, suggesting that DPYSL2-mediated localization of WAVE1 is critical for axon formation (Kawano et al., 2005). As it is known that lncRNAs bind to proteins to promote their localization (X. Zhang et al., 2019), it is likely that the m^{6}A mark on *Malat1* acts as a beacon for WAVE complex proteins. Once bound, *Malat1* may coordinate the localization of these proteins to form complexes and, ultimately, influence synapse and spine formation and maintenance. Therefore, our RNA-MS data suggest that m^{6}A-modified *Malat1* contributes to the consolidation of fear-extinction memory through RBP interactions and protein localization.

Finally, we found that targeted degradation and demethylation of m^{6}A-*Malat1* led to impaired fear-extinction memory. Many previous studies on m^{6}A in the brain relied on the manipulation of m^{6}A methyltransferases and demethylases (Widagdo et al., 2016; Walters et al., 2017; Koranda et al., 2018; Shi et al., 2018) with very few examining the effect of manipulating a single RNA at a specific time and place (X. M. Liu and Qian, 2021). To address this within the context of fear extinction, we used the CIRTS-YTHDF2/CIRTS-FTO single plasmid system (Rauch et al., 2018) with the inclusion of a Calm3 intronic region to localize the construct to the synapse in an activity-dependent manner (Sharangdhar et al., 2017; Liau, 2022). Indeed, site-specific and activity-dependent degradation of *Malat1* at the synapse using CIRTS-YTHDF2 resulted in the impairment of fear-extinction memory. This effect was also observed after targeted demethylation of *Malat1* at the synapse using CIRTS-FTO, suggesting that m^{6}A-modified *Malat1* is critical for the consolidation of fear-extinction memory. The impairment in the consolidation of fear-extinction memory is likely because of a reduction in dendritic spine formation because of targeted demethylation of *Malat1* at the synapse. Together, our findings highlight a critical role of m^{6}A in regulating the functional state of RNA during memory consolidation and expand the repertoire of memory-related m^{6}A readers in the synaptic compartment.

References

Alarcón C, Goodarzi H, Lee H, Liu X, Tavazoie S, Tavazoie S (2015) HNRNPA2B1 is a mediator of m6A-dependent nuclear RNA processing events. Cell 162:1299–1308.

Alberini CM (2009) Transcription factors in long-term memory and synaptic plasticity. Physiol Rev 89:121–145.

Alon S, et al., IMAXT Consortium (2021) Expansion sequencing: spatially precise in situ transcriptomics in intact biological systems. Science 371: eaax2656.

Bai L, Tang Q, Zou Z, Meng P, Tu B, Xia Y, Cheng S, Zhang L, Yang K, Mu S, Wang X, Qin X, Lv B, Cao X, Qin Q, Jiang X, Chen C (2018) m6A demethylase FTO regulates dopaminergic neurotransmission deficits caused by arsenite. Toxicol Sci 165:431–446.

Barry G (2014) Integrating the roles of long and small noncoding RNA in brain function and disease. Mol Psychiatry 19:410–416.

Bernard D, Prasanth KV, Tripathi V, Colasse S, Nakamura T, Xuan Z, Zhang MQ, Sedel F, Jourdren L, Coulpier F, Triller A, Spector DL, Bessis A (2010) A long nuclear-retained noncoding RNA regulates synaptogenesis by modulating gene expression. EMBO J 29:3082–3093.

Briggs JA, Wolvetang EJ, Mattick JS, Rinn JL, Barry G (2015) Mechanisms of long noncoding RNAs in mammalian nervous system development, plasticity, disease, and evolution. Neuron 88:861–877.

Bruel-Jungerman E, Davis S, Laroche S (2007) Brain plasticity mechanisms and memory: a party of four. Neuroscientist 13:492–505.

Chen B, Brinkmann K, Chen Z, Pak CW, Liao Y, Shi S, Henry L, Grishin NV, Bogdan S, Rosen MK (2014) The WAVE regulatory complex links diverse receptors to the actin cytoskeleton. Cell 156:195–207.

Chen X, Yu C, Guo M, Zheng X, Ali S, Huang H, Zhang L, Wang S, Huang Y, Qie S, Wang J (2019) Down-regulation of m6A mRNA methylation is involved in dopaminergic neuronal death. ACS Chem Neurosci 10:2355–2363.

Chen Z, Borek D, Padrick SB, Gomez TS, Metlagel Z, Ismail AM, Umetani J, Billadeau DD, Otwinowski Z, Rosen MK (2010) Structure and control of the actin regulatory WAVE complex. Nature 468:533–538.

Coker H, Wei G, Brockdorff N (2019) m6A modification of noncoding RNA and the control of mammalian gene expression. Biochim Biophys Acta Gene Regul Mech 1862:310–318.

Davenport E, Szulc B, Drew J, Taylor J, Morgan T, Higgs N, López-Doménech G, Kittler J (2019) Autism and schizophrenia-associated CYFIP1 regulates the balance of synaptic excitation and inhibition. Cell Rep 26:2037–2051.e6.

De Rubeis S, Pasciuto E, Li KW, Fernández E, Di Marino D, Buzzi A, Ostroff LE, Klann E, Zwartkruis FJ, Komiyama NH, Grant SG, Poujol C, Choquet D, Achsel T, Posthuma D, Smit AB, Bagni C (2013) CYFIP1 coordinates mRNA translation and cytoskeleton remodeling to ensure proper dendritic spine formation. Neuron 79:1169–1182.

Dominissini D, Moshitch-Moshkovitz S, Schwartz S, Salmon-Divon M, Ungar L, Osenberg S, Cesarkas K, Jacob-Hirsch J, Amariglio N, Kupiec M, Sorek R, Rechavi G (2012) Topology of the human and mouse m6A RNA methylomes revealed by m6A-seq. Nature 485:201–206.

Edens BM, Vissers C, Su J, Arumugam S, Xu Z, Shi H, Miller N, Rojas Ringeling F, Ming GL, He C, Song H, Ma YC (2019) FMRP modulates neural differentiation through m6A-dependent mRNA nuclear export. Cell Rep 28:845–854.e5.

Fu Y, Zhuang X (2020) m6A-binding YTHDF proteins promote stress granule formation. Nat Chem Biol 16:955–963.

Godbout M, Erlander MG, Hasel KW, Danielson PE, Wong KK, Battenberg EL, Foye PE, Bloom FE, Sutcliffe JG (1994) 1G5: a calmodulin-binding, vesicle-associated, protein kinase-like protein enriched in forebrain neurites. J Neurosci 14:1–13.

Grabinski TM, Kneynsberg A, Manfredsson FP, Kanaan NM (2015) A method for combining RNAscope in situ hybridization with immunohistochemistry in thick free-floating brain sections and primary neuronal cultures. PLoS One 10:e0120120.

He R, Jiang J, Luo D (2020) The functions of N^6-methyladenosine modification in lncRNAs. Genes Dis 7:598–605.

Hendrickson GD, Kelley DR, Tenen D, Bernstein B, Rinn JL (2016) Widespread RNA binding by chromatin-associated proteins. Genome Biol 17:28.

Hess ME, Hess S, Meyer KD, Verhagen LA, Koch L, Brönneke HS, Dietrich MO, Jordan SD, Saletore Y, Elemento O, Belgardt BF, Franz T, Horvath TL, Rüther U, Jaffrey SR, Kloppenburg P, Brüning JC (2013) The fat mass and obesity associated gene (Fto) regulates activity of the dopaminergic midbrain circuitry. Nat Neurosci 16:1042–1048.

Hou ST (2020) The regulatory and enzymatic functions of CRMPs in neuritogenesis, synaptic plasticity, and gene transcription. Neurochem Int 139:104795.

Huang H, et al. (2018) Recognition of RNA N^6-methyladenosine by IGF2BP proteins enhances mRNA stability and translation. Nat Cell Biol 20:285–295.

Ito H, Atsuzawa K, Morishita R, Usuda N, Sudo K, Iwamoto I, Mizutani K, Katoh-Semba R, Nozawa Y, Asano T, Nagata K (2009) Sept8 controls the binding of vesicle-associated membrane protein 2 to synaptophysin. J Neurochem 108:867–880.

Jia G, Fu Y, Zhao X, Dai Q, Zheng G, Yang Y, Yi C, Lindahl T, Pan T, Yang YG, He C (2011) N^6-methyladenosine in nuclear RNA is a major substrate of the obesity-associated FTO. Nat Chem Biol 7:885–887.

Kawano Y, Yoshimura T, Tsuboi D, Kawabata S, Kaneko-Kawano T, Shirataki H, Takenawa T, Kaibuchi K (2005) CRMP-2 is involved in kinesin-1-dependent transport of the Sra-1/WAVE1 complex and axon formation. Mol Cell Biol 25:9920–9935.

Ke S, Alemu E, Mertens C, Gantman E, Fak J, Mele A, Haripal B, Zucker-Scharff I, Moore M, Park C, Vagbo C, Kussnierczyk A, Klungland A, Darnell J, Darnell R (2015) A majority of m^{6}A residues are in the last exons, allowing the potential for 3′ UTR regulation. Genes Dev 29:2037–2053.

Kim Y, Sung JY, Ceglia I, Lee KW, Ahn JH, Halford JM, Kim AM, Kwak SP, Park JB, Ho Ryu S, Schenck A, Bardoni B, Scott JD, Nairn AC, Greengard P (2006) Phosphorylation of WAVE1 regulates actin polymerization and dendritic spine morphology. Nature 442:814–817.

Koranda J, Dore L, Shi H, Patel MJ, Vaasjo LO, Rao MN, Chen K, Lu Z, Yi Y, Chi W, He C, Zhuang X (2018) Mettl14 is essential for epitranscriptomic regulation of striatal function and learning. Neuron 99:283–292.e5.

Krishnamoorthy K, Thomson J (2004) A more powerful test for comparing two Poisson means. Stat Plan Infer 119:23–35.

Kroll J, Özçete Ö, Jung S, Maritzen T, Milosevic I, Wichmann C, Moser T (2020) AP180 promotes release site clearance and clathrin-dependent vesicle reformation in mouse cochlear inner hair cells. Cell Sci 133: jcs236737.

Liau WS (2022) Fear extinction is regulated by long noncoding RNA activity at the synapse. bioRxiv 486308. https://doi.org/10.1101/2022.03.30.486308.

Lin Q, Wei W, Coelho CM, Li X, Baker-Andresen D, Dudley K, Ratnu VS, Boskovic Z, Kobor MS, Sun YE, Bredy TW (2011) The brain-specific microRNA miR-128b regulates the formation of fear-extinction memory. Nat Neurosci 14:1115–1117.

Liu N, Parisien M, Dai Q, Zheng G, He C, Pan T (2013) Probing N^6-methyladenosine RNA modification status at single nucleotide resolution in mRNA and long noncoding RNA. RNA 19:1848–1856.

Liu N, Dai Q, Zheng G, He C, Parisien M, Pan T (2015) N^6-methyladenosine-dependent RNA structural switches regulate RNA-protein interactions. Nature 518:560–564.

Liu N, Zhou K, Parisien M, Dai Q, Diatchenko L, Pan T (2017) N^6-methyladenosine alters RNA structure to regulate binding of a low-complexity protein. Nucleic Acids Res 45:6051–6063.

Liu XM, Qian SB (2021) Targeted RNA m6A editing using engineered CRISPR-Cas9 conjugates. In: RNA modifications: methods and protocols (McMahon M, ed), pp 399–414. New York: Springer.

Madugalle SU, Meyer K, Wang DO, Bredy TW (2020) RNA N^6-methyladenosine and the regulation of RNA localization and function in the brain. Trends Neurosci 43:1011–1023.

Makihara H, Nakai S, Ohkubo W, Yamashita N, Nakamura F, Kiyonari H, Shioi G, Jitsuki-Takahasi A, Nakamura H, Tanaka F, Akase T, Kolattukudy P, Goshima Y (2016) CRMP1 and CRMP2 have synergistic but distinct roles in dendritic development. Genes Cells 21:994–1005.

Mao Y, Dong L, Liu X, Guo J, Ma H, Shen B, Qian S (2019) m6A in mRNA coding regions promotes translation via the RNA helicase-containing YTHDC2. Nat Commun 10:5332.

Marsden KC, Jain RA, Wolman MA, Echeverry FA, Nelson JC, Hayer KE, Miltenberg B, Pereda AE, Granato M (2018) A Cyfip2-dependent excitatory interneuron pathway establishes the innate startle threshold. Cell Rep 23:878–887.

Martin SJ, Grimwood PD, Morris RG (2000) Synaptic plasticity and memory: an evaluation of the hypothesis. Annu Rev Neurosci 23:649–711.

Matsuoka Y, Li X, Bennett V (1998) Adducin is an in vivo substrate for protein kinase C: phosphorylation in the MARCKS-related domain inhibits activity in promoting spectrin-actin complexes and occurs in many cells, including dendritic spines of neurons. J Cell Biol 142:485–497.

Meng J, Cui X, Rao MK, Chen Y, Huang Y (2013) Exome-based analysis for RNA epigenome sequencing data. Bioinformatics 29:1565–1567.

Merkurjev D, Hong WT, Iida K, Oomoto I, Goldie BJ, Yamaguti H, Ohara T, Kawaguchi SY, Hirano T, Martin KC, Pellegrini M, Wang DO (2018) Synaptic N^6-methyladenosine (m6A) epitranscriptome reveals functional partitioning of localized transcripts. Nat Neurosci 21:1004–1014.

Meyer KD, Saletore Y, Zumbo P, Elemento O, Mason CE, Jaffrey SR (2012) Comprehensive analysis of mRNA methylation reveals enrichment in 3′UTRs and near stop codons. Cell 149:1635–1646.

Pathania M, Davenport EC, Muir J, Sheehan DF, López-Doménech G, Kittler JT (2014) The autism and schizophrenia associated gene CYFIP1 is critical for the maintenance of dendritic complexity and the stabilization of mature spines. Transl Psychiatry 4:e374.

Przyborowski J, Wilenski H (1940) Homogeneity of results in resting samples from Poisson series: with an application to testing clover seed for dodder. Biometrika 31:313–323.

Rauch S, Chuan H, Dickinson B (2018) Targeted m6A reader proteins to study epitranscriptomic regulation of single RNAs. J Am Chem Soc 140:11974–11981.

Rauch S, He E, Srienc M, Zhou H, Zhang Z, Dickinson BC (2019) Programmable RNA-guided RNA effector proteins built from human parts. Cell 178:122–134.e12.

Roundtree I, Luo G, Zhang Z, Wang X, Zhou T, Cui Y, Sha J, Huang X, Guerrero L, Xie P, He E, Shen B, He C (2017) YTHDC1 mediates nuclear export of N^6-methyladenosine methylated mRNAs. Elife 6:e31311.

Sala C, Piëch V, Wilson NR, Passafaro M, Liu G, Sheng M (2001) Regulation of dendritic spine morphology and synaptic function by Shank and Homer. Neuron 31:115–130.

Selth LA, Gilbert C, Svejstrup JQ (2009) RNA immunoprecipitation to determine RNA-protein associations in vivo. Cold Spring Harbor, NY: Cold Spring Harbor Laboratory.

Sharangdhar T, Sugimoto Y, Heraud-Farlow J, Fernández-Moya SM, Ehses J, Ruiz de los Mozos I, Ule J, Kiebler MA (2017) A retained intron in the 3′-UTR of Calm3 mRNA mediates its Staufen2- and activity-dependent localization to neuronal dendrites. EMBO Rep 18:1762–1774.

Shi H, et al. (2018) m6A facilitates hippocampus-dependent learning and memory through YTHDF1. Nature 563:249–253.

Soderling SH, Guire ES, Kaech S, White J, Zhang F, Schutz K, Langeberg LK, Banker G, Raber J, Scott JD (2007) A WAVE-1 and WRP signaling complex regulates spine density, synaptic plasticity, and memory. J Neurosci 27:355–365.

Spadaro PA, Flavell CR, Widagdo J, Ratnu VS, Troup M, Ragan C, Mattick JS, Bredy TW (2015) Long noncoding RNA-directed epigenetic regulation of gene expression Is associated with anxiety-like behavior in mice. Biol Psychiatry 78:848–859.

Takenawa T, Suetsugu S (2007) The WASP-WAVE protein network: connecting the membrane to the cytoskeleton. Nat Rev Mol Cell Biol 8:37–48.

Walters BJ, Mercaldo V, Gillon CJ, Yip M, Neve RL, Boyce FM, Frankland PW, Josselyn SA (2017) The role of The RNA demethylase FTO (fat mass and obesity-associated) and mRNA methylation in hippocampal memory formation. Neuropsychopharmacology 42:1502–1510.

Wang X, Zhao B, Roundtree I, Lu Z, Han D, Ma H, Weng X, Chen K, Shi H, He C (2015) N^6-methyladenosine modulates messenger RNA translation efficiency. Cell 161:1388–1399.

Wei W, Zhao Q, Wang Z, Liau WS, Basic D, Ren H, Marshall PR, Zajaczkowski EL, Leighton LJ, Madugalle SU, Musgrove M, Periyakaruppiah A, Shi J, Zhang J, Mattick JS, Mercer TR, Spitale RC, Li X, Bredy TW (2022) ADRAM is an experience-dependent long noncoding RNA that drives fear extinction through a direct interaction with the chaperone protein 14-3-3. Cell Rep 38:110546.

Widagdo J, Zhao QY, Kempen MJ, Tan MC, Ratnu VS, Wei W, Leighton L, Spadaro PA, Edson J, Anggono V, Bredy TW (2016) Experience-dependent accumulation of N^6-methyladenosine in the prefrontal cortex is associated with memory processes in mice. J Neurosci 36:6771–6777.

Xiao W, et al. (2016) Nuclear m^{6}A reader YTHDC1 regulates mRNA splicing. Mol Cell 61:507–519.

Xiao Y, Wang Y, Tang Q, Wei L, Zhang X, Jia G (2018) An elongation- and ligation-based qPCR amplification method for the radiolabeling-free detection of locus-specific N-6-methyladenosine modification. Angew Chem Int Ed Engl 57:15995–16000.

Yoshimura T, Kawano Y, Arimura N, Kawabata S, Kikuchi A, Kaibuchi K (2005) GSK-3β regulates phosphorylation of CRMP-2 and neuronal polarity. Cell 120:137–149.

Zhang H, Kang E, Wang Y, Yang C, Yu H, Wang Q, Chen Z, Zhang C, Christian KM, Song H, Ming G-l, Xu Z (2016) Brain-specific Crmp2 deletion leads to neuronal development deficits and behavioural impairments in mice. Nat Commun 7:11773.

Zhang J, Zhao B, Zhu X, Li J, Wu F, Li S, Gong X, Cha C, Guo G (2018) Phosphorylation and SUMOylation of CRMP2 regulate the formation and maturation of dendritic spines. Brain Res Bull 139:21–30.

Zhang X, Hamblin MH, Yin KJ (2017) The long noncoding RNA Malat1: its physiological and pathophysiological functions. RNA Biol 14:1705–1714.

Zhang X, Wang W, Zhu W, Dong J, Cheng Y, Yin Z, Shen F (2019) Mechanisms and functions of long non-coding RNAs at multiple regulatory levels. Int J Mol Sci 20:5573.

Zhang Y, Lee Y, Han K (2019) Neuronal function and dysfunction of CYFIP2: from actin dynamics to early infantile epileptic encephalopathy. BMB Rep 52:304–311.

Zhang Z, Wang M, Xie D, Huang Z, Zhang L, Yang Y, Ma D, Li W, Zhou Q, Yang Y, Wang X (2018) METTL3-mediated N^6-methyladenosine mRNA modification enhances long-term memory consolidation. Cell Res 28:1050–1061.

Zhou J, Wan J, Shu XE, Mao Y, Liu XM, Yuan X, Zhang X, Hess ME, Brüning JC, Qian SB (2018) N^6-methyladenosine guides mRNA alternative translation during integrated stress response. Mol Cell 69:636–647. e637.

Zhou KI, Shi H, Lyu R, Wylder AC, Matuszek Ż, Pan JN, He C, Parisien M, Pan T (2019) Regulation of co-transcriptional pre-mRNA splicing by m^{6}A through the low-complexity protein hnRNPG. Mol Cell 76:70–81. e79.